The Institute of Paper Chemistry

Appleton, Wisconsin

Doctor's Dissertation

The Development of Apparatus and Techniques for the Study of the Dielectric Constant and Loss Angle of Paper

Cyril H. Delevanti, Jr.

May, 1943

THE DEVELOPMENT OF APPARATUS AND TECHNIQUES FOR THE STUDY OF THE DIELECTRIC CONSTANT AND LOSS ANGLE OF PAPER

A thesis submitted by

Cyril H. Delevanti, Jr.

B.S. in Ch.E. 1938, The Rice Institute

M.S. 1941, Lawrence College

in partial fulfillment of the requirements of The Institute of Paper Chemistry for the degree of Doctor of Philosophy from Lawrence College, Appleton, Wisconsin

May, 1943

TABLE OF CONTENTS

INTRODUCTION

Substances are classified in three general groups according to their electrical conductivity—namely, metallic conductors, semiconductors, and insulators or dielectrics. At room temperatures, metallic conductors usually have a conductivity of 10^3 mho cm.$^{-1}$ or greater. If the conductivity of a substance is less than 10^{-10} mho cm.$^{-1}$, it is classed as a dielectric. Dry cellulose has a conductivity of the order of 10^{-15} mho cm.$^{-1}$ and, therefore, is classed as a dielectric. The substances in the intermediate group are called semiconductors.

No substance is a perfect dielectric, because there is always a dissipation of power when a dielectric is subjected to an electrical stress. Among the best dielectrics from the standpoint of low dielectric loss are amber, mica, transformer oil, glass, quartz, air, silk, certain of the synthetic resins, and rubber. Dry wood, paper, and cotton are somewhat less efficient, although the last two find extensive application in modern industry by reason of certain desirable physical and chemical properties and their economic availability.

The application of paper as an insulating material is as old as the electrical industry itself. The annual consumption of paper for high-voltage cable insulation alone is of the order of 5000 tons. In spite of many limitations, impregnated paper has proved itself by far the superior material for the insulation of high voltage cables. The impregnated paper cable cannot be approached in performance by any other type, and without it the remarkable expansion in transmission and distribution of electric power would still be in a

very primitive stage.

It has been found experimentally that the dielectric constant of an impregnated paper cannot be accurately estimated from the dielectric constant of its components. It appears that the impregnating compounds act as if they formed a series rather than a parallel circuit with the paper. A consequence is that any gain in capacity obtainable by increasing the dielectric constant of the impregnant is limited by the dielectric constant of the paper sheet. Any research giving additional information as to the factors affecting the dielectric constant of paper would be of great interest in this field.

In addition to the 5000 tons of paper used annually for high-voltage cable insulation, an approximately equal quantity of cellulosic insulation is employed in each of the four other types of insulation—namely, telephone cables, textile insulation, paper capacitors, and reinforced and laminated insulation in which cellulose is used as the reinforcing material in thermoplastic resins.

DEFINITION OF TERMS

Before passing to a specific discussion of the dielectric properties of cellulose, the terms used in describing the electrical properties of a dielectric will be discussed.

Dielectric Constant. The dielectric constant of a dielectric material is that property which determines the electrostatic energy stored in the material per unit volume per unit potential gradient.

Dielectric Phase Angle. The dielectric phase angle is the angular difference in phase between the sinusoidal voltage applied to the dielectric and the component of the resulting current which has the same frequency as the applied voltage.

Dielectric Loss Angle. The dielectric loss angle is the difference between 90 electrical degrees and the dielectric phase angle. A clearer picture of the relation of the phase angle and loss angle will be obtained by inspection of the vector diagram in Figure 1 for an imperfect capacitor showing power loss.

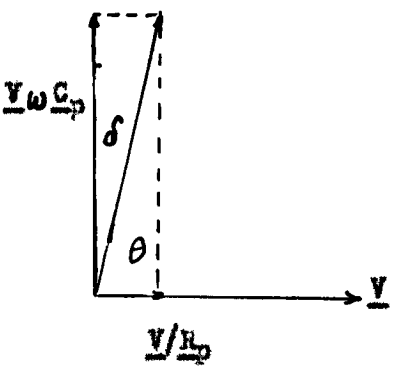

Figure 1

In Figure 1,

$\underline{V}$ = the voltage applied to the capacitor,

ω = 2 π x frequency,

$\underline{C}_p$ = the equivalent parallel capacitance,

$\underline{R}_p$ = the equivalent parallel resistance,

δ = the dielectric loss angle, and

θ = the dielectric phase angle.

In any electrical circuit the power dissipated is given by the equation

$$\underline{P} = \underline{V}\,\underline{I} \cos\theta,$$

where

$\underline{V}$ = the voltage,

$\underline{I}$ = the current, and

$\cos\theta$ = the power factor, which is the cosine of the phase angle.

In Figure 1, when θ is large and, consequently, δ is small, it is found that

$$\tan\delta \approx \delta \approx \cos\theta \approx 1/(\underline{R}_p\,\underline{C}_p\,\omega) = \tan\delta$$

or the power factor ($\cos\theta$) is approximately equal to the loss angle (δ) in radians. In fact, when $\tan\delta$ is less than 0.1, the error is less than 0.005 if the power factor is taken as $1/\underline{R}_p\,\underline{C}_p\,\omega$. The approximation $\tan\delta = \delta$ when δ is small is so close that, throughout this investigation, δ will be considered as equal to $1/\underline{R}_p\,\underline{C}_p\,\omega$.

Dielectric Loss Factor. The dielectric loss factor of a material is the product of its dielectric constant and the tangent of its loss angle. The power loss per unit volume of an insulating material at a stated frequency, voltage gradient, and temperature is proportional to its dielectric loss factor.

Dielectric Strength. The dielectric strength of a material is the voltage gradient at which the material breaks down and loses its insulating properties. A study of dielectric strength was not carried out in this investigation, but a definition of the term is included as it is often confused with dielectric constant.

Leakage Conductance. Leakage conductance is the reciprocal of the volume resistivity as measured by experimental means permitting of correction for surface conductivity.

CELLULOSE AS A DIELECTRIC

The physical and chemical properties of cellulose enable it to be used in a large variety of forms having a remarkable range of dielectric properties. For example, the dielectric constant of cellulose in its purest form is exceptionally high for a solid dielectric (approximately 7). It also has physical properties which enable it to be used in a form having a very low dielectric constant (only slightly greater than one). Its power factor over a wide range of frequencies is a small fraction of 1 per cent, and its resistivity, when well dried, is of the order of 10^{16} ohm cm. Its dielectric strength is higher than that of most dielectrics, reaching values of the order of 2.5×10^{6} volts $cm.^{-1}$ in thin films. In addition to this remarkable combination of dielectric properties, it has an unusual combination of other physical and chemical properties such as high chemical stability, the ability to withstand elevated temperatures, and a high tensile strength and flexibility in thin films.

Direct Current Phenomena

For cellulose, as for most solid dielectrics, the observed current for a given temperature and field intensity does not remain constant but decreases for some time after the field has been applied. It is common practice, therefore, to express the conductivity of cellulose in terms of the current flowing after 1 minute of application

of potential. Yet most of this current is not a true ionic conduction current and, even after much longer periods of application of potential, most of it is reversible. This behavior is responsible for the fact that under alternating fields absorption phenomena are dependent upon the frequency.

When a potential difference is applied to a dry sheet of paper, the current changes with time according to the equation

$$I = k\, t^{-n},$$

where

I = the current,

k = a constant,

t = the time after the application of potential, and

n = a constant.

Some dielectrics, such as impregnated paper insulation, show some departure from the t^{-n} expression. It has not been possible to determine the current at very small intervals after the application of voltage, but the exponential relationship of current and time indicates that it rises rapidly as t approaches 0. At ordinary temperatures, the steady-state value of the current may be reached only after several hours or even days and may be as low as 10^{-4} of that observed initially.

If the specimen is short circuited, it is found that a current, known as the discharging current, flows in the reverse direction. If the steady-state current has been reached before short circuiting, the discharge current shows essentially the same variation with time as the charging current.

The decrease of current with time is attributed to the building up of a counter e.m.f. of polarization within the dielectric. This polarization e.m.f. can be detected by measuring the potential difference across the dielectric after the external field has been removed. The values of the polarization e.m.f. increase with time very rapidly immediately after application of an external voltage, but later decrease less rapidly and eventually become constant. It has also been found that the limiting polarization e.m.f. is proportional to the applied voltage.

Alternating Current Phenomena

The anomalous behavior of solid dielectrics in an alternating field was first noticed in 1864 by von Siemens, who observed that considerable heat was developed in certain dielectrics when subjected to an alternating stress. The alternating losses in solid dielectrics are due almost entirely to the phenomena of absorption, losses due to conductivity being very small compared with those resulting from the absorption, and there is no evidence of losses of other types. In the case of cellulose, it has been found experimentally that the direct current conductivity is sufficient to account for only about 1 per cent of the alternating current conduction in the dry state.

From the standpoint of engineering practice, absorption is generally represented in effect as a conduction phenomenon; when an alternating stress is applied to a dielectric, there is a component of current in phase with the applied voltage. This means an energy loss in the dielectric. In the field of communication by telegraphy

and telephony, these losses cause attenuation, damping, and confusion of signals and speech. It is because of these energy losses that the use of the paper capacitor is excluded in high frequency work and finds its greatest use at commercial power frequencies, although large capacitors can be seriously deteriorated at such frequencies by undissipated heat energy. In the field of high voltage transmission, where impregnated paper cable is used almost exclusively, the absorption loss causes heating and danger to the life of the insulation.

HISTORICAL REVIEW

It has not been attempted to cover comprehensively in this section the extensive literature relating to the electrical behavior of cellulose and cellulose products both in alternating and direct current fields, but rather to establish a background for this investigation and to accquaint the reader in a general way with researches which have been conducted in this field. If a greater insight is desired, especially in the field of dielectric strength, electrical resistance of cellulose, and the dielectric properties of various cellulose derivatives, the reader is referred to the very interesting and comprehensive reviews prepared annually by the Committee on Chemistry, Conference on Electrical Insulation of the National Research Council.

TEST METHODS FOR THE ELECTRICAL CHARACTERISTICS OF PAPER

The inherent electrical characteristics of a dielectric (such as paper) are dielectric strength, loss angle, dielectric constant, and leakage conductance. Tentative methods of test for power factor and dielectric constant of electrical materials are outlined by the American Society for Testing Materials (1). These methods describe the various types of electrical bridges adapted to the measurement of the dielectric constant and power factor of insulating materials, and contain literature references for each type of circuit.

De Lucs, Campbell, and Hauss (2) have devised a method for measuring the dielectric constant of a material which cannot be made to fill a capacitor completely. In their method, two completely

miscible liquids are so chosen that the dielectric constant of the material under examination lies between the two values for the liquids. A curve is drawn showing the relation between dielectric constant and the percentage composition of the two liquids. A second curve is drawn showing this relation for the liquids and fibrous material. The intersection gives the composition of that liquid which has the same dielectric constant as the fibrous material. This method is applicable to paper pulp.

Strength properties, such as tear and tensile, are extremely important for insulating papers, because these papers are quite frequently subjected to mechanical stress in their application to the apparatus and during the use of the finished product. Porosity and absorption are also important properties, especially if the paper product is to be impregnated with oil. Tentative methods of testing untreated paper used in electrical insulation have been outlined by the American Society for Testing Materials (3). Methods of physical testing are given, and an apparatus is described for determining the number of conducting particles per unit area of the paper.

A tentative method of test for the dielectric strength of insulating materials at commercial power frequencies is outlined by the American Society for Testing Materials (4).

THE CHEMICAL NATURE OF CELLULOSE AS A DIELECTRIC

Kohman (5) has published an excellent paper describing the behavior of cellulose as a dielectric in both alternating and direct

current fields. He made a study of the charge and discharge currents of paper dielectrics with time and showed that there is a reversible flow of current. Kohman has also given curves for the dielectric constant and power factor versus temperature for several frequencies, showing a low temperature region of power factor dispersion for dry paper and an increase in capacity with an increase in temperature or decrease in frequency.

Several investigators have studied the effect of moisture content on the dielectric properties of paper. Argue and Maass (6) measured the variation of the dielectric constants of cellulosic materials containing various amounts of adsorbed water. They found that the dielectric constant of the water initially adsorbed is less than one-quarter that of liquid water, but it increases with the amount subsequently adsorbed until the dielectric constant approaches that of liquid water as the water content of the fiber approaches the fiber saturation point.

Whitehead and Greenfield (7) investigated the dielectric loss, phase angle, and capacitance of paper specimens as related to the moisture content. They arrived at the following relationships:

(a) The total capacitance varies approximately as an exponential function of the moisture content.

(b) The component of total geometric capacitance attributable to occluded water varies directly with the water content.

(c) The component of capacitance resulting from dielectric absorption, the total power factor, and the absorption component of power factor all vary as exponential functions of the moisture content.

(d) The conduction component of power factor varies as an exponential function of the moisture content only in the lower ranges, increasing thereafter more rapidly and no longer in simple relation.

Greenfield (3) found that dried cable paper shows a regular decrease in dielectric absorption with a decrease in moisture. Equations are described for calculating from dielectric measurements small amounts of moisture absorbed. Greenfield has also given curves of power factor and capacity for different periods of drying (the pressure being decreased from 760 mm. to 0.25 mm. in five steps), showing a regular decrease in power factor and capacity at 100° C. as the drying pressure is reduced.

Race, Hemhill, and Endicott (9), in making electrical measurements on paper, mounted test electrodes with paper in place in a desiccator and dried the sample for 16 hours at 100° C. and at a pressure of 10^{-3} mm. of mercury. At the end of the drying period, thoroughly dried air was admitted and electrical measurements were made as the temperature dropped. They found a decrease in power factor as the temperature decreased. It is claimed by Barton (10) that, for temperatures as low as 60° C., paper can be brought to a state of complete dryness by circulation of air at atmospheric pressure. Reduction of pressure, although it accelerates the process, does not change the final electrical properties of the paper. Whitehead and Greenfield (11) studied the relation of the dielectric properties of paper to temperature and found that, over the range of 20° to 100° C., there is little change in the measured dielectric constant or in the geometric dielectric constant of dry paper. Within the

upper range of temperature, a slight decrease in these values was observed, which they attributed to a decrease in the density caused by thermal expansion of the dielectric.

THE ELECTRICAL RESISTANCE OF CELLULOSE

McLean and Kohman (12) presented data showing the dependence of apparent direct-current conductivity upon the moisture content of paper, the potential gradient, and the time of application of potential. At moisture contents below 1 per cent, a steady decrease in current with time occurs; at 1 to 3 per cent moisture, the initial decrease is followed by a strong increase in apparent conductivity with time and voltage. At moisture contents above 3 per cent, current was found to decrease with time.

In studying the dependence of the conductivity of dry paper on temperature and voltage, Murphy and McLean (13) found that for dry paper the logarithm of resistivity falls sharply with increasing temperature. These authors also stated that, in drying paper for resistance measurements, the water evolved comes in part from the evaporation of adsorbed water and in part from thermal decomposition of the paper.

Seborg and Stamm (14) found that log (1/R) increases linearly with the percentage of moisture up to the fiber saturation point. Beyond the fiber saturation point, log (1/R) changes little with the percentage of moisture. Weidmann (15) found a hysteresis of moisture and resistance for ascending and descending humidities.

DIELECTRIC STRENGTH OF CELLULOSE

Although a study of dielectric strength was not included in this investigation, several interesting points have been noticed in reading the literature of this field.

Whitehead (16) found from accelerated voltage time tests on impregnated paper that the 60-cycle breakdown voltage decreased with increasing thickness of several layers of paper tape (about 25 per cent on increasing the thickness from 3 to 8 mills). The decrease in life was approximately 45 per cent. Power factor and dielectric loss decreased with increasing thickness of paper tape, the former by 30 per cent and the latter by 20 per cent over the range of thickness studied.

THE EFFECT OF CERTAIN IMPURITIES ON THE DIELECTRIC PROPERTIES OF CELLULOSE

Vogel (17) discussed several properties of cable paper and condenser paper which influence dielectric behavior, anddescribed test methods for physical strength, oil absorption, power factor, and breakdown strength. In studies of power factor as a function of temperature, a sharp break in power factor was found for most papers above 75° C. This increase was shown to depend to a large extent upon the presence of electrolytic impurities. These impurities were found to decrease the rate of drying considerably.

The results of sorption experiments carried out by Piper, Kerstein, and Fleiger (18) confirm the hypothesis that the oil-soluble organic acids of low molecular weight which cause marked increase in

power factor of impregnated paper are strongly sorbed by the paper. High molecular weight acids have no effect and are not sorbed. Shanklin (19) produced an improvement in the insulation of high voltage cables by washing the paper with pure water and removing the residual air by treatment with carbon dioxide. The improvement is demonstrated by curves showing the results of power factor tests. McLean (20) found that most of the ash could be removed from insulating paper only by extraction with dilute acids such as 0.01 N hydrochloric acid. Washing with distilled water alone is not sufficient.

According to Finch (21), the use of chloride-contaminated paper in fine coil windings is to be avoided. A condenser made of paper purposely contaminated with 0.19 per cent of a chloride failed in about 1.5 hours under exaggerated conditions of increased direct-current voltage, one made of paper containing 0.03 per cent of chlorides failed in 60 hours, and one with 0.01 per cent failed after 240 hours. It was observed that the ability of condenser paper to withstand exposure to heat was dependent upon the absence of acids or acid salts. It was also found that the insulation resistance was impaired by moisture, Cl, OH, NH_4, and SO_3 ions from the cooking and bleaching processes, and by resinates from rosin sizing.

Konagata (22) has devised an electro-washing (electrodialysis) process. Samples of the original kraft, sodium pulp, pulp taken before the paper machine, and the finished paper were tested. Handsheets were prepared from the electro-washed samples and the electrical and mechanical properties determined. It was found that the best condenser paper was produced by electro-washing after the beating process.

THE DIELECTRIC PROPERTIES OF REGENERATED CELLULOSE AND OF VARIOUS CELLULOSE DERIVATIVES

Hartshorn and Rushton (23) discussed comprehensively the dielectric behavior of cellulose acetate and compared it with that of paper. Their work was confined to cellulose acetate with a 2 per cent power factor. Absorption of water from the atmosphere increased the power factor; it also increased with increasing frequency and decreased with the temperature. The dielectric properties of cellophane have been reported by Stoops (24). He also studied a sample of almost pure cellulose triacetate and found that the change in composition over cellophane (pure cellulose) lowered the dielectric constant nearly 50 per cent. Hill (25) has given power factor versus frequency curves for cellophane, cellulose acetate, and cellulose nitrate, and found that cellulose nitrate had a higher power factor at the lower frequencies than either cellulose acetate or cellophane. He suggested the possibility of sealing safety glass by heat developed directly by high frequency losses in the cellulose material. Campbell (26) reported a value of 6.7 for the dielectric constant of regenerated cellulose.

PRESENTATION OF PROBLEM

The main purpose of this investigation was to develop a suitable apparatus and techniques for determining the dielectric constant and loss angle of paper samples in the dry state.

The main features of the apparatus were to include (1) a test capacitor with guard ring contained in a chamber capable of evacuation to very low pressures for drying the paper sample; (2) an electrode arrangement whereby the electrodes can be separated in vacuo to permit drying of the paper sample and can then be brought together for taking electrical measurements, and (3) a suitable bridge arrangement and auxiliary apparatus for measuring the dielectric constant and loss angle of paper samples.

The techniques to be developed included (1) a method of preparing test specimens; (2) a technique for drying the specimens to constant electrical properties; and (3) methods for making such measurementsas thickness of the specimen and electrode separation as required for the computation of dielectric constant and loss angle.

Because it is difficult to reproduce accurately the density of a handsheet, it was desired to know the functional relationship between density and the dielectric constant and loss angle so that samples could be corrected to some standard density for purposes of comparison. Furthermore, because a material such as paper cannot be made to fill completely a parallel plate test capacitor, it was necessary to develop a satisfactory theory for the interpretation of the measured dielectric constant and loss angle of the test capacitor.

APPARATUS USED

The circuit used for the determination of equivalent parallel capacitance and loss angle of a test capacitor using paper as a dielectric was the conjugate Schering bridge, incorporating the desirable features of the Wagner ground, as described in the A.S.T.M. standards on tests for power factor and dielectric constant (1). A.S.T.M. describes this circuit as follows:

"..... this bridge is applicable for all frequencies from 25 cycles per second up to 1 megacycle per second. R_3 and R_4 [referring to Figure 7 of the article] shall be identical resistor units of a type practically free from capacitance, with resistance of the order of 10,000 ohms for use at frequencies of 10 kilocycles per second and less; 1000-ohm units may be used for frequencies of the order of 1 megacycle per second if the capacity of the source warrants. The air capacitor, C_3, is used to produce a positive reading for C_4 and C_2 alone is in the circuit; it should be no larger than is necessary for this purpose."

The circuit used is essentially that shown in Figure 7 of the A.S.T.M. standard (1), using the 10,000-ohm resistors for frequencies of 10 kilocycles $sec.^{-1}$ and less, except that the bridge shielding was extended to include the leads to the bridge detector and the fixed capacitor C_3 specified by A.S.T.M. was replaced by a variable air capacitor. The bridge circuit with the changes mentioned is shown in Figure 2, the heavy lines representing the bridge circuit and the light lines the shielding. In the following section, the individual bridge

Figure 2

Conjugate Schering Bridge Circuit

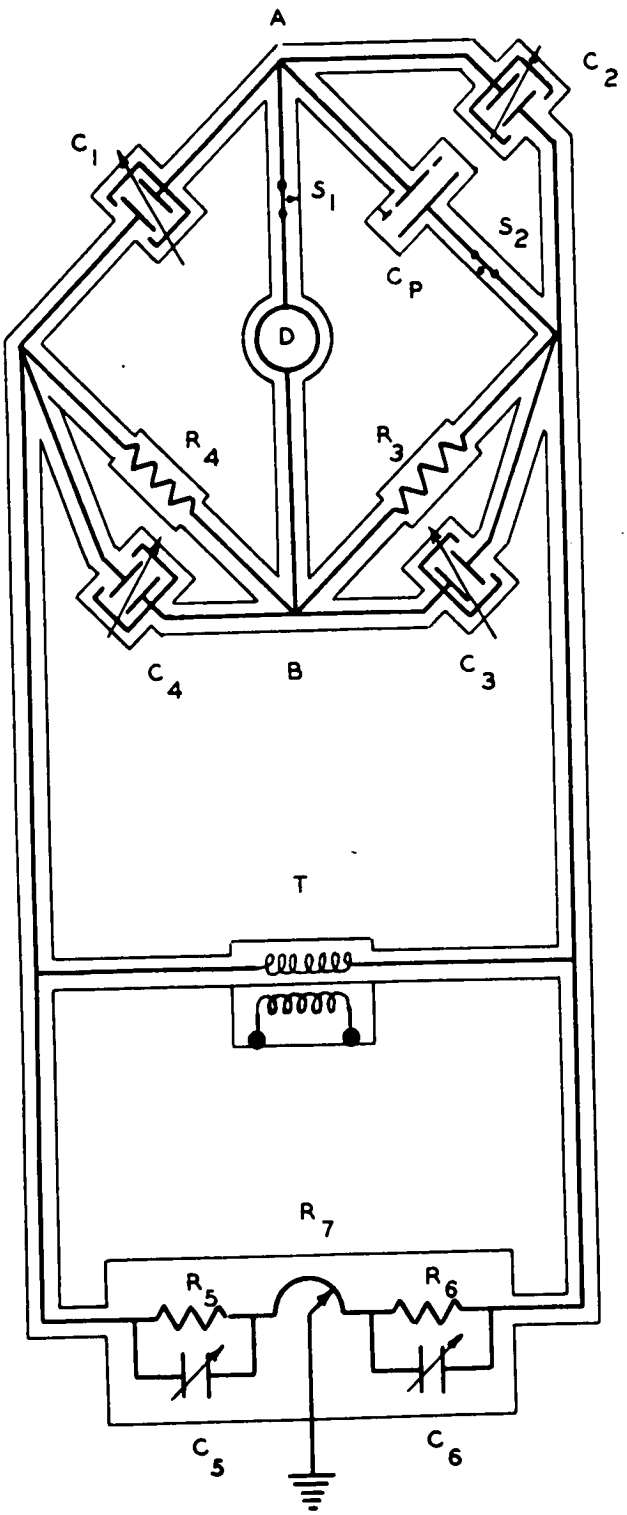

elements and auxiliary apparatus used will be discussed.

THE OSCILLATOR

All measurements of dielectric constant and loss angle in this investigation were made at 1000 cycles sec.$^{-1}$ by using a General Radio audio oscillator Type 213-B to supply the input voltage to the bridge. The audio oscillator is contained in the shield box A, shown in Figure 3. A 6-volt lead storage battery was used to energize the oscillator, and the alternating voltage of 4.2 volts supplied by the low voltage terminals of the audio oscillator was found sufficient to operate the bridge at a satisfactory sensitivity.

THE ISOLATION TRANSFORMER

The output of the audio oscillator energizes the primary winding of a 1 to 4.5 turns ratio, shielded isolation transformer shown at B in Figure 3. The transformer was manufactured by the Thordarson Company according to the following specifications:

Primary coil - 50 ohms impedance at 50 cycles sec.$^{-1}$.
Secondary coil - approximately 1000 ohms impedance.
Turns ratio - approximately 1 to 4.5.
Both primary and secondary coils individually shielded.
Maximum capacity between windings and shields - 200 mmfds.
Maximum capacity between shields - 30 mmfds.
Maximum capacity between windings - 30 mmfds.
Complete transformer to be mounted on nickel alloy steel.

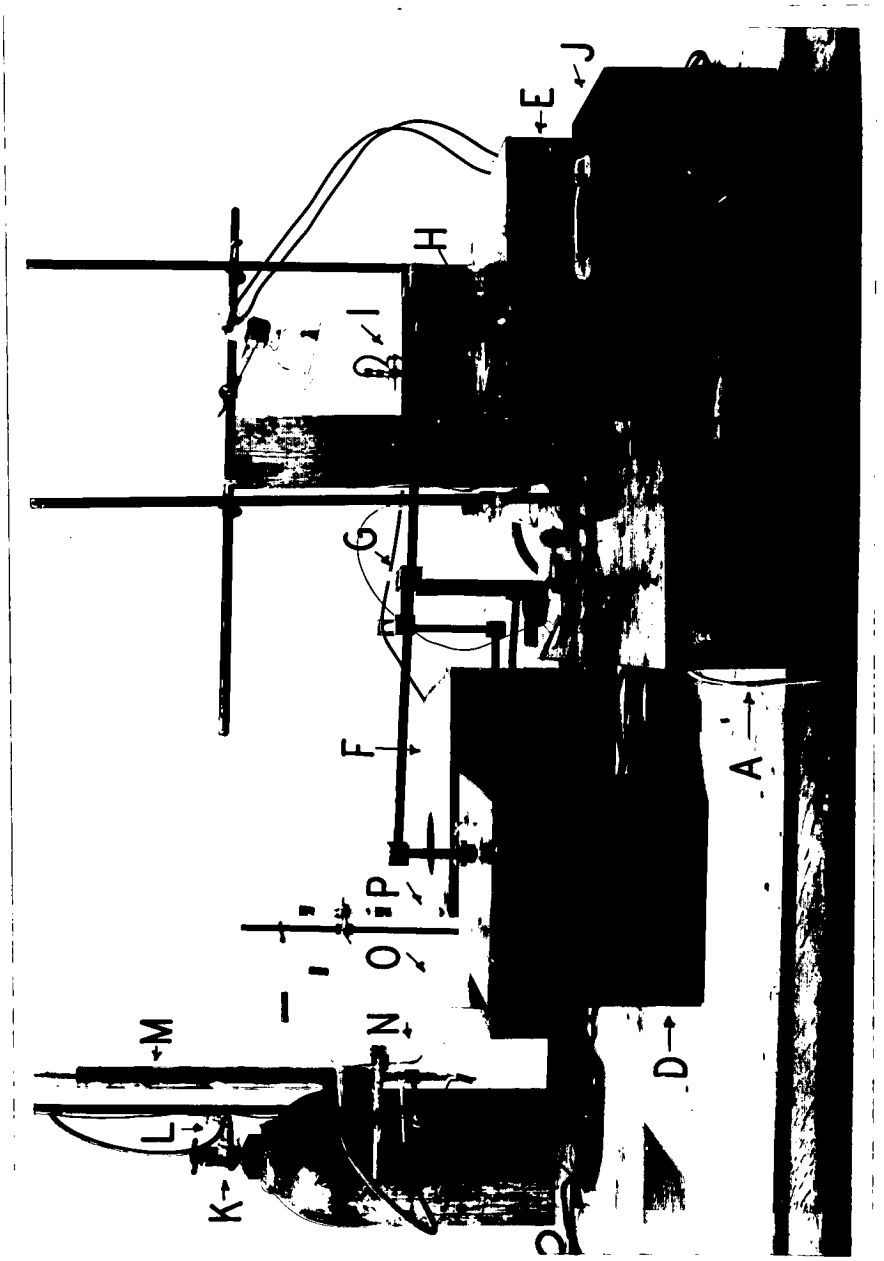

Figure 3

Apparatus Used for the Determination of
the Dielectric Constant and Loss Angle of Paper

The secondary windings of the isolation transformer are conducted to the bridge box C (see Figure 3).

The connection between the individual bridge units contained in shield boxes was made by No. 30 enameled copper wire led through 1/2-inch copper shield tubes. Right angle bends and joints were made by soldering the shield tubes to small copper connecting boxes. To hold the conducting wires concentric with the shield tubes, polystyrene plugs were cemented to the ends of the shield tubes inside the connecting boxes and the wire pulled taut through small holes drilled in the center of the plugs. The shield tubes and connecting boxes are plainly seen in Figure 3.

CHECKING THE CAPACITIVE CONSTANTS OF THE ISOLATION TRANSFORMER

The bridge arrangement shown in Figure 4 was used to check the capacitive constants of the isolation transformer.

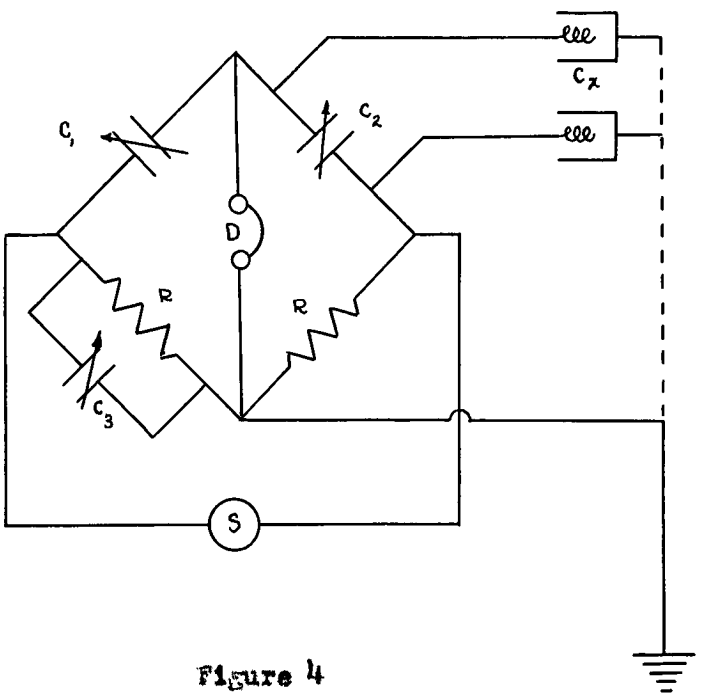

Figure 4

The following circuit constants were used in the bridge arrangement of Figure 4:

$\underline{S}$ = 1000 cycles sec.$^{-1}$ audio oscillator

$\underline{C_1}$ = General Radio Type 246-L capacitor

$\underline{C_2}$ = General Radio Type 722-D precision capacitor

$\underline{C_3}$ = 0-500-mmfd. variable air capacitor

$\underline{C_x}$ = isolation transformer

$\underline{R}$ = 10,000 ohms

$\underline{D}$ = headphone detector

The various capacitive constants of the isolation transformer were determined by the method of substitution against the precision capacitor $\underline{C_2}$. The results are given in Table I.

TABLE I

CAPACITIVE CONSTANTS OF THE ISOLATION TRANSFORMER

Capacity between windings	negligible
Capacity of secondary to shield	344 mmfds.
Capacity of primary to shield	240 mmfds.
Capacity between windings with shield floating	74 mmfds.
Capacity between shields	65 mmfds.

By the use of the isolation transformer with the low capacity between windings, the bridge is electrostatically shielded from its input, a necessary condition for satisfactory operation, incidentally giving the bridge flexibility in that it can be operated by sources of alternating voltage unsymmetrical with respect to ground potential.

CONSTRUCTION OF THE BRIDGE BOX

The bridge box, shown at C in Figure 3, contains the Wagner ground connection, capacitors C_4 and C_3, and the resistors R. Attention is called to the drawing of the electrical circuit of the bridge (Figure 2) for identifying the various circuit elements.

A bottom view of the bridge box is shown in Figure 5. The two 100-mmfd. variable air capacitors C_5 and C_6, the matched pair of resistors R_5 and R_6, and the 25-ohm potentiometer R_7 comprise the Wagner ground elements and are contained in the lower shield compartment shown in Figure 5. The capacitors C_5 and C_6 are supported by polystyrene posts secured to the top panel. These capacitors are adjusted by levers above the panel through polystyrene rods coupled to the rotors of the capacitors.

S_1 and S_2 (Figure 5) are shields for the matched resistors R_3 and R_4, respectively (Figure 2). All shielding is grounded as a part of the metal bridge box except S_3 and S_4 (Figure 5) which are shields for the 100-mmfd. variable air capacitors C_3 and C_4, respectively (Figure 2). This shielding is fastened to polystyrene posts which support capacitors C_3 and C_4, and so remains electrically insulated from the ground. The rotors of the capacitors C_3 and C_4 are connected to their respective shields S_3 and S_4. The common point of connection to shields S_3 and S_4 and resistors R_3 and R_4 is led through conduit 4 (Figure 5) to the bridge detector and constitutes point B in Figure 2.

As the capacitor C_4 is the only element in the bridge box whose setting appears in the equation for δ (Equation 2, page 34), it is

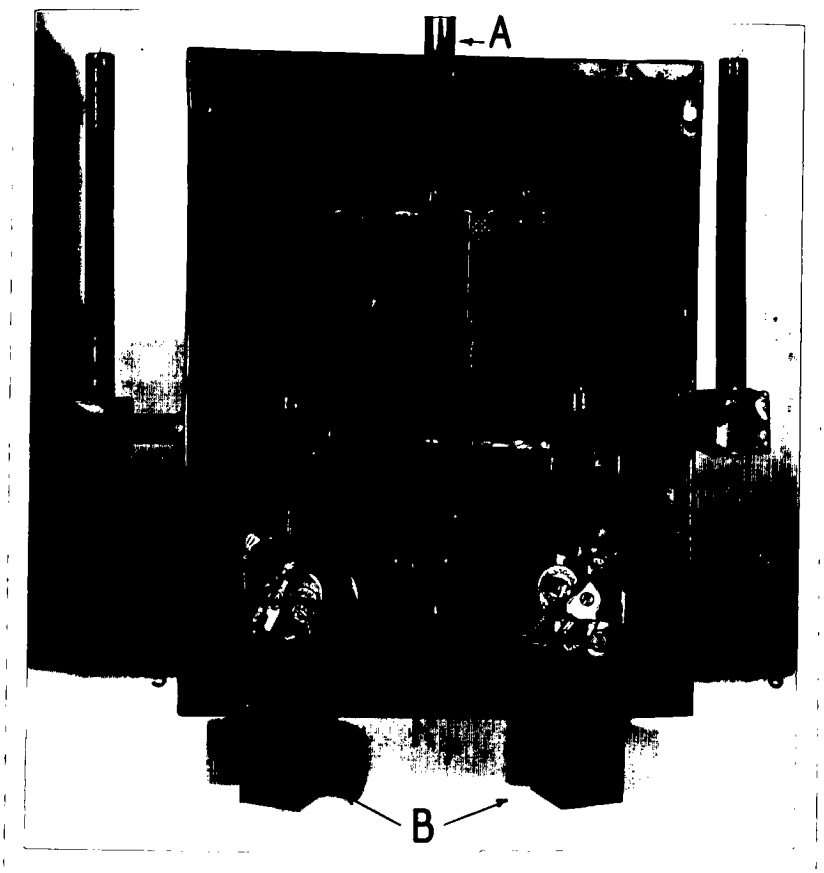

Figure 5

Bottom View of the Bridge Box

adjusted accurately by a vernier dial connected to its rotor by a polystyrene rod. The capacitor C_3 is adjusted by a knob connected to its rotor by a polystyrene rod.

The wiring of the Wagner ground connection, as well as the wiring to capacitors C_3 and C_4, was made quite heavy to give the parts added mechanical rigidity. The rotors of each capacitor were adjusted to turn smoothly, because it was found that transient effects caused by sticking rotors seriously interfered with the precise adjustment of the bridge.

Isolantite-insulated air capacitors and polystyrene insulation were chosen to keep losses to a minimum.

Conduits B (Figure 5) lead to the isolation transformer T (Figure 2), and conduits C and D lead to capacitors C_1 and C_2, respectively (Figure 2).

Checking of the Matched Resistors

The 10,000-ohm matched pairs of resistors R_3, R_4, and R_5, R_6 (Figure 2) were checked with a General Radio impedance bridge Type 650-A and found to have negligible distributed inductance and capacity, and a resistance close to 10,000 ohms.

It is important to the operation of the bridge that the four resistors be paired. A check on the resistance matching was obtained with the Wheatstone bridge arrangement shown in Figure 6, using two decade resistance boxes R_a and R_b, a pair of matched resistors R_c and R_d, and a sensitive galvanometer G.

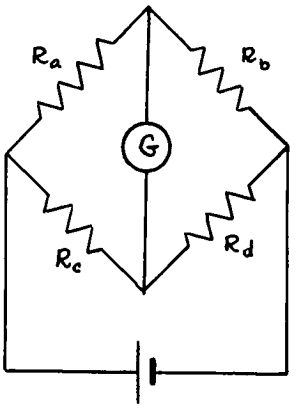

Figure 6

In taking data, R_a was held constant over two readings for a pair. The second reading was obtained with the resistors at R_c and R_d interchanged. The results given in Table II were obtained.

TABLE II

CHECKING OF MATCHED RESISTORS

R_a ohms	R_b ohms	R_c	R_d
990.0	989.7	R_6	R_5
990.0	990.0	R_5	R_6
990.0	990.0	R_3	R_4
990.0	989.8	R_4	R_3

At bridge balance,

$$R_a R_4 = R_b R_c.$$

and, for the pair of resistors R_5 and R_6,

$$R_a R_5 = R_b R_6. \text{ and}$$

$$R_a R_6 = R_b' R_5.$$

Then,

$$R_5/R_6 = \sqrt{R_b/R_b'} = \sqrt{989.7/990.0} = 0.9998.$$

Similarly,

$$R_3/R_4 = R_b/R_b' = 989.8/990.0 = 0.9999.$$

The resistors then pair to about one part in 10,000.

Calibration of the Capacitor C_4

The shield S_4 and connections to the capacitor C_4 were opened, and the capacitor was calibrated in place in the central bridge box (Figure 5). The circuit arrangement shown in Figure 7 was employed in the calibration.

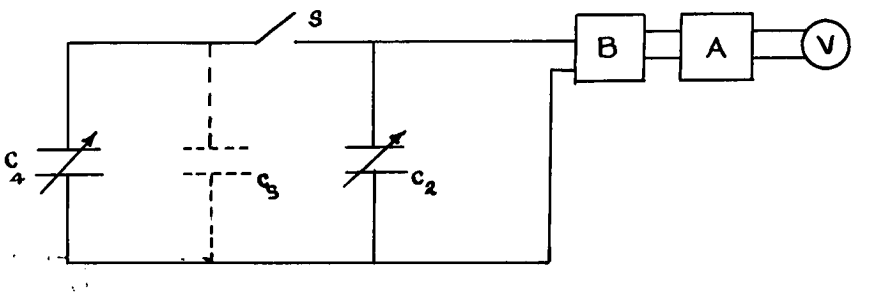

Figure 7

In Figure 7, C_4 represents the capacitor to be calibrated, C_2 the General Radio Type 722-D precision capacitor, and C_s small stray capacitances. The General Radio impedance bridge Type 650-A is represented by B, and the General Radio amplifier Type 514-A by A with its output voltmeter V. The impedance bridge used has an internal source of e.m.f. at 1000 cycles $sec.^{-1}$, and, hence, the calibration of C_4 was made at this frequency. The following procedure—i.e., the method of substitution—was used.

First, the bridge was balanced as indicated by V with the switch S open and the precision capacitor set at some value C_2. With

the unknown capacitor set at some value C_4, the switch S was closed and balance again obtained by adjustment of the precision capacitor to a value C_2'. Then,

$$C_4 + C_s = C_2 - C_2'.$$

By varying the dial setting of the unknown to obtain a value C_4',

$$C_4 = (C_4' - C_4) = \Delta(C_2 - C_2').$$

Because in the bridge equation used for the computation of δ (see Equation 2, page 54) only ΔC_4 is of interest, absolute values of the capacitance C_4 are not necessary. Changes in C_s only shift the calibration curve to the right or left. The data given in Table III were obtained for the calibration of the capacitor C_4 at 1000 cycles $sec.^{-1}$.

TABLE III

CALIBRATION DATA FOR CAPACITOR C_4

C_2 mmfds.	C_2' mmfds.	Dial Reading	$C_4 + C_s$ mmfds.
499.8	381.6	100.0	118.2
	389.5	90.0	110.3
	402.0	80.0	97.8
	414.1	70.0	85.7
	425.5	60.0	74.3
	436.5	50.0	63.3
	447.0	40.0	52.8
	458.6	30.0	41.2
	470.6	20.0	29.2
	482.0	10.0	17.8
	486.8	0.0	13.0

The data given in Table III are plotted in Figure 8. From this calibration curve, it is found that, for dial readings between 90.0 and 10.0,

Figure 5

$G_1 + G_2$ vs. Dial Reading
at 1000 Cycles $Sec.^{-1}$

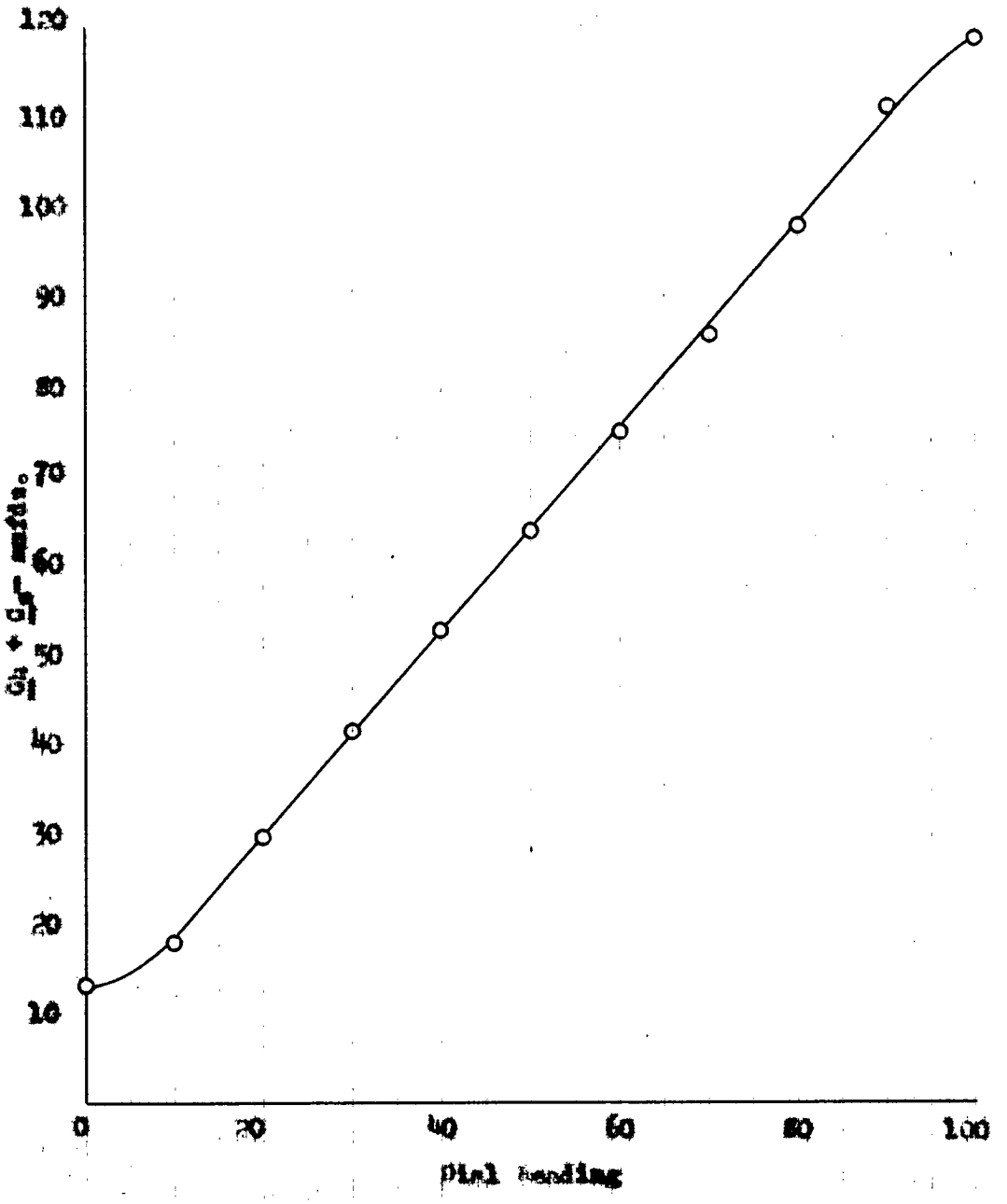

$\Delta C_4 = \Delta$Dial Reading (109 - 18)/(90 - 10) $= \Delta$Dial Reading x 1.14.

THE REFERENCE CAPACITOR AND THE PRECISION CAPACITOR

The reference capacitor C_1 (Figure 2) is a 0-1500-mmfd. General Radio Type 246-L variable air capacitor. The figure of merit $R\omega C^2$ given by the manufacturer is 0.06×10^{-12} at 1000 cycles sec.$^{-1}$. Because C_1 serves as a reference capacitor, its calibration need not be known and it is necessary only that it have low electrical losses and a capacitance range comparable with that of capacitor C_2 (see Figure 2).

The shield box for capacitor C_1 is shown at D in Figure 3. The capacitor C_1 is adjusted by a knob outside the shield connected to the rotor reducing gear by a polystyrene rod.

The precision capacitor C_2 (Figure 2) is a General Radio Type 722-D precision capacitor. This capacitor is built in two sections, the high section having a terminal capacitance of 100 to 1100 mmfds. and the low section a terminal capacitance of 25 to 110 mmfds. The high section only was used in this work. As the absolute values of the capacitor C_2 are required in the computation of the loss angle and C_p (see Equation 1 and 2, page 54), it is necessary that C_2 be a capacitor of known calibration and low electrical losses. The terminal capacitance of C_2 of the high section, as read by the instrument drum and dial, is guaranteed to $\pm$ 1 mmfd. accuracy, and differences can be read to at least 0.1 mmfd. The figure of merit $R\omega C^2$ for each section at 1000 cycles sec.$^{-1}$ is given by the manufacturer as better than 0.04×10^{-12} and is approximately constant with setting.

The shield box for capacitor C_2 is shown at E in Figure 3. The capacitor C_2 is adjusted by a knob outside the shield box connected to the rotor worm drive by a polystyrene rod. Drum and dial readings of C_2 are observed through a screened window cut in the top of the shield box.

The rotors of capacitors C_1 and C_2 are connected to a copper lining inside their wooden cases. Because the rotors are at ground potential only at bridge balance, any undue leakage to the ground is avoided by standing the capacitors on glass plates inside the shield boxes.

THE BRIDGE BALANCE INDICATOR

A three-stage, battery-operated, vacuum tube amplifier with an alternating current output voltmeter was used as a null indicator for balancing the bridge. In order to eliminate the difficulties inherent in alternating-current operated, high gain amplifiers, the type 1N5-G vacuum tube was selected for each stage because of its low direct-current filament voltage and high amplification factor.

The circuit diagram for the amplifier is given in Figure 9; the circuit constants are as follows:

R_1 = 0.25-megohm potentiometer gain control
R_2 = 0.25 megohms
R_3 = 0.6 megohms
R_4 = 1 megohm
C_1 = 0.03 mfd.
C_2 = 0.02 mfd.
C_3 = 1 mfd.
V = 0-2-volt alternating current output voltmeter, 20,000 ohms resistance

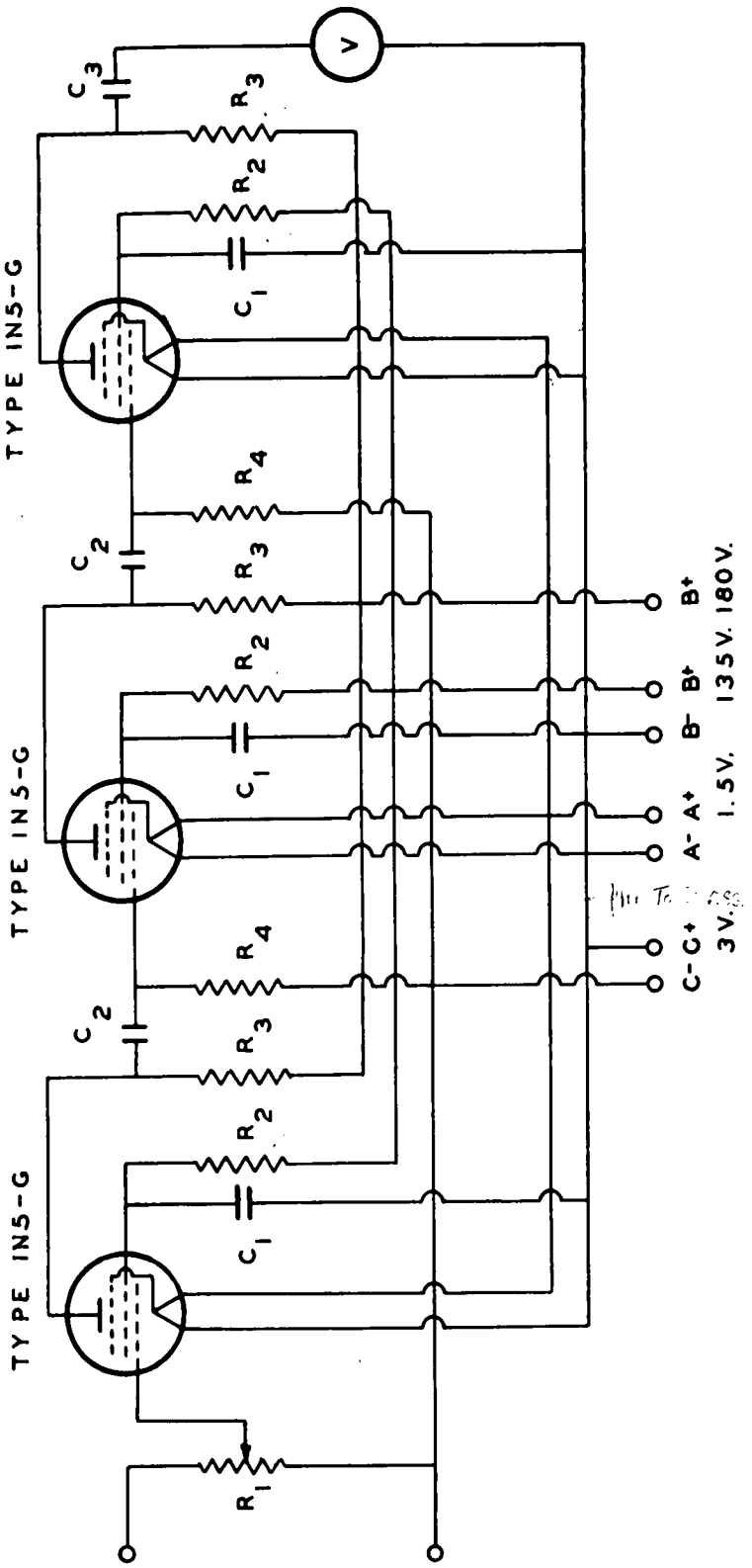

Figure 9

Circuit Diagram of the Bridge Balance Detector

The amplifier, batteries, and output meter are contained in the shield box F shown in Figure 3. The lid of the shield box is provided with a screened window for viewing the output meter. The amplifier is assembled on a metal chassis and provided with interstage shielding. Because the input terminals of the amplifier are at ground potential only when the bridge is correctly balanced, it is necessary to insulate all component parts of the amplifier from the ground. To insure this the amplifier chassis, batteries, and output meter are supported on a glass plate inside the shield. The glass plate in turn rests on sponge rubber pads inside the shield to reduce microphonic effects.

Measurement of the Voltage Gain of the Amplifier

The voltage gain of the amplifier was determined by the following method. The low voltage output of the 1000 cycles $sec.^{-1}$ audio oscillator, General Radio Type 213-B, was shunted by a 2-megohm and a 500-ohm resistor in series as shown in Figure 10.

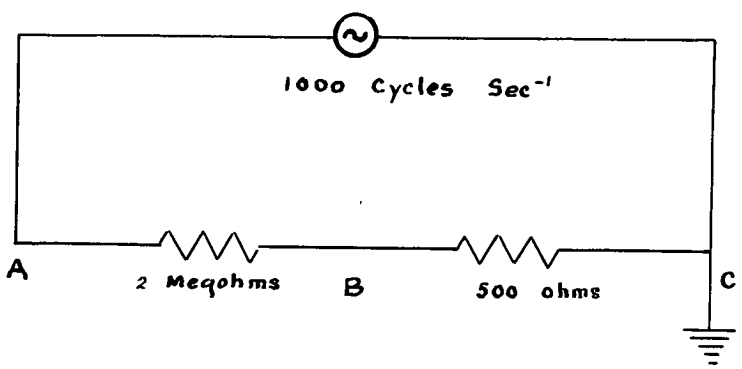

Figure 10

The potential drop from A to C was 4.2 volts and that from B to C was 1.1×10^{-3} volt. Points B and C were connected to the input

of the amplifier, and the output signal voltage was observed with a cathode ray oscillograph. To calibrate the oscillograph, its gain control was adjusted to give a reasonable signal amplitude with the oscillograph input connected to points A and B, and the amplitude of the signal was measured on the fluorescent screen. The oscillograph sweep circuit was not used, giving the signal the appearance of a vertical straight line. Without changing the gain setting, the oscillograph was connected to the amplifier output (the amplifier input being connected to points B and C, and the signal amplitude was again measured. Knowing the potential difference A to B and B to C, it is possible to compute the voltage gain of the amplifier by assuming the length of the vertical line on the fluorescent screen to be proportional to impressed signal voltages at small amplitudes.

The maximum voltage gain obtained for the amplifier with its output meter disconnected was 1.8×10^4; it was 8.5×10^3 with the output meter connected.

Using the various amplifier circuit constants and assuming small hypothetical variations in voltage on the control grid, a theoretical voltage gain, u, for the given conditions as calculated from R.C.A. data (27) is 110. In a resistance coupled amplifier such as that under discussion, the load impedance of the tube is approximately equal to the resistance of the plate resistor in parallel with the grid resistor of the following stage. If R_p is the plate resistor and R_g is the grid resistor in the following stage, the actual voltage gain per stage may be written as $(R_g/(R_p + R_g))\ u$, where u is the theoretical voltage gain for the tube under the given conditions of operation.

Theoretically (disregarding all other losses), the factor $k = R_g/(R_p + R_g)$ for the first two stages should be 1/1.6 = 0.63. In the last stage, the value for k is unfavorably small. Whereas the plate resistor is 600,000 ohms, the impedance of the voltmeter is only 20,000 ohms. The gain of the last stage, therefore, is 0.0323 u. Considering the gain of the last stage as 0.0323 u, k = 0.45 for the first two stages as calculated from the maximum gain of 8.5×10^3 obtained for the amplifier with the output meter connected. It would seem that the difference between this factor (0.45) and the theoretical one (0.63) could be accounted for by losses and improper choice from the tube manual of the theoretical amplification factor.

SWITCHES S_1 AND S_2

Two high impedance shielded switches S_1 and S_2 (Figure 2) are required. Switch S_1 is shown at G and S_2 at H in Figure 3. Switch S_1 was constructed as shown in Figure 11.

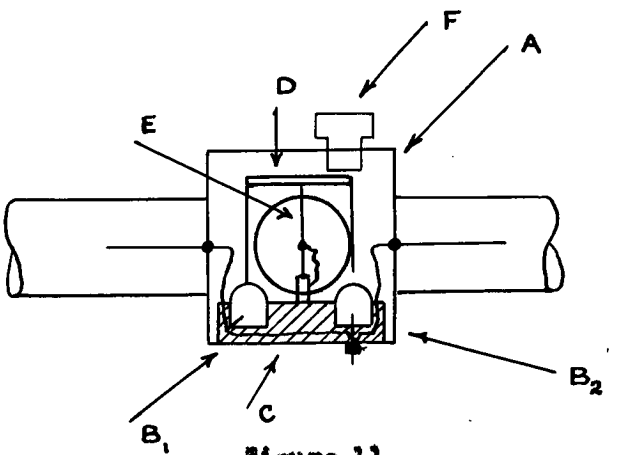

Figure 11

Switch S_1 is contained in the 1-inch cube copper connecting box A in Figure 11. Two wells B_1 and B_2 were drilled in a slab of

insulating polystyrene C. In well B_1, a contact wire was admitted through a small hole in the polystyrene and sealed in place with polystyrene cement. A machine screw was fastened through the bottom of well B_2, serving the purpose of a ground contact and holding the polystyrene slab to the connecting box. Both wells were filled with a drop of mercury to serve as contact points with cross member D, which was soldered to a short length of clock spring E. For the switch S_1, the cross member D is connected to the amplifier and well B_1 is connected to the common point A (Figure 2). When the polystyrene button F is depressed, the amplifier is connected to the ground; when pressure on the button is released, the clock spring restores contact of the amplifier to the common point A (Figure 2).

THE TEST CAPACITOR

The test capacitor consists of an upper electrode A, a lower electrode B, and guard ring C shown in the top and side views in the drawing (Figure 12). The three electrodes were machined from 1/4-inch brass plate to the dimensions shown in Figure 12.

The guard ring was cut away at the top surface to narrow the effective radial width to 0.068 inch. This was done to decrease the capacitance of the guard ring to the upper electrode. The reason for so doing is discussed under the equivalent electrical circuit of the bridge. A.S.T.M. (1) states empirically that the radial width of the guard ring should not be less than five times the separation of the electrodes. The guard ring width, therefore, allows the accurate testing of samples up to 0.014 inch in thickness. Holes were drilled and

Figure 12

Top and Side Views of the Test Capacitor

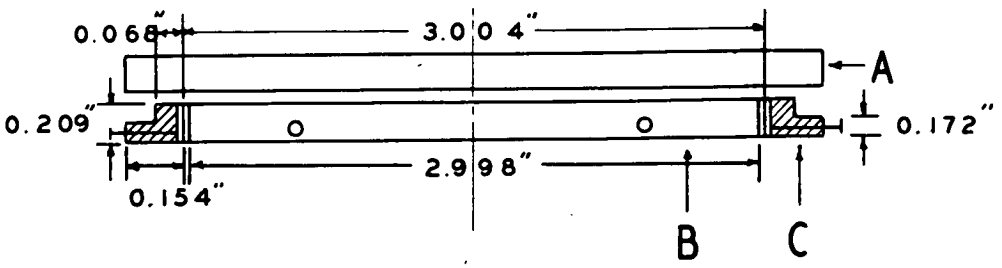

Side View - Upper and Lower Electrode

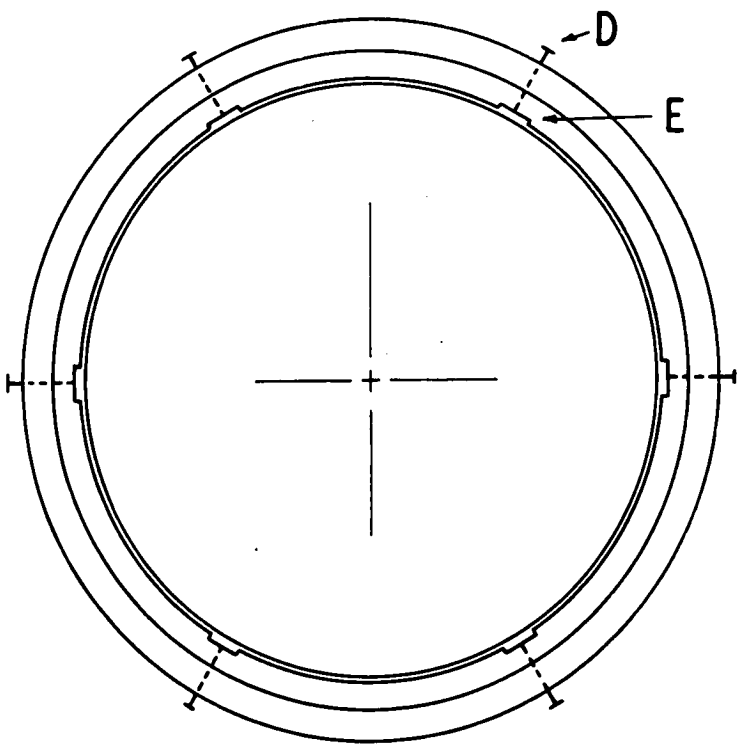

Top View - Lower Electrode

tapped at 60-degree intervals around the guard ring to accommodate set screws D. Small slots about 1/4 inch deep and 3/16 inch wide were cut into the inner periphery of the guard ring at the set screws to allow for a reasonable thickness of supporting dielectric between the set screws and the lower electrode.

The lower electrode and guard ring were held coplanar against a piece of plate glass and waxed in place at the back preparatory to the grinding operation. To avoid distorting the surfaces of the electrodes from a true plane, as usually happens in adopting ordinary grinding methods, the lower electrode-guard ring combination and the upper electrode were ground smooth and plane on an optical jig by the Riggs Optical Company, Appleton, Wisconsin. The polished electrodes were given a light platinum plating by a method outlined in the Chemical Formulary (28). The finished electrodes were buffed lightly with white rouge.

To assemble the guard ring and lower electrode, both were laid with the polished surface down on a piece of plate glass and centered by inserting small mica strips split to about 0.003 inch in the clearance between the guard ring and lower electrode. The slots E were packed with several thicknesses of mica strips and the two electrodes firmly clamped to the glass plate. The set screws D were then uniformly tightened to maintain centering between the two electrodes. The mica spacers inserted in the guard ring clearance for centering were removed and the two electrodes tested with a steel straight edge against a strong light to make sure they were coplanar.

The guard ring clearance was made as large as 0.003 inch to avoid the difficulties experiences in maintaining good insulation when smaller clearances were tried. One layer of mica 0.003 inch thick could have been used as insulation between the set screws and the lower test electrode, omitting the slots E. This was tried but it did not prove successful. The slots decrease the effectiveness of the guard ring somewhat, but the correction is considered negligible because the area cut out by the slots is small as compared with the total effective area of the guard ring. The resistance between the guard ring and lower electrode obtained by the use of several thicknesses of mica supporting dielectric is of the order of 10^9 ohms. This resistance is not high when compared with good insulation resistance but it is large when compared with the bridge impedance of 10^4 ohms to the ground, and thus no disturbance of the bridge sensitivity is to be expected close to the balance point.

THE TEST CHAMBER AND SHIELD

The shielded test chamber is shown at I in Figure 3, and a drawing showing details is given in Figure 13. The base plate A (Figure 13) was of heavy brass plate and was fastened to the shield box B by pillars C. Half-inch holes were drilled in the base plate over lead-in seals D soldered to the base plate. The lead-in seals were sawed-off ends of grid-cap type metal vacuum tubes, which were found satisfactory from the standpoint of vacuum tightness and high dielectric quality. Connection was made to the lead-in seal by inserting a tinned loop of no. 22 copper wire through the hole in the base plate, holding it against the short wire leading through the glass

Figure 13

The Test Chamber and Shield

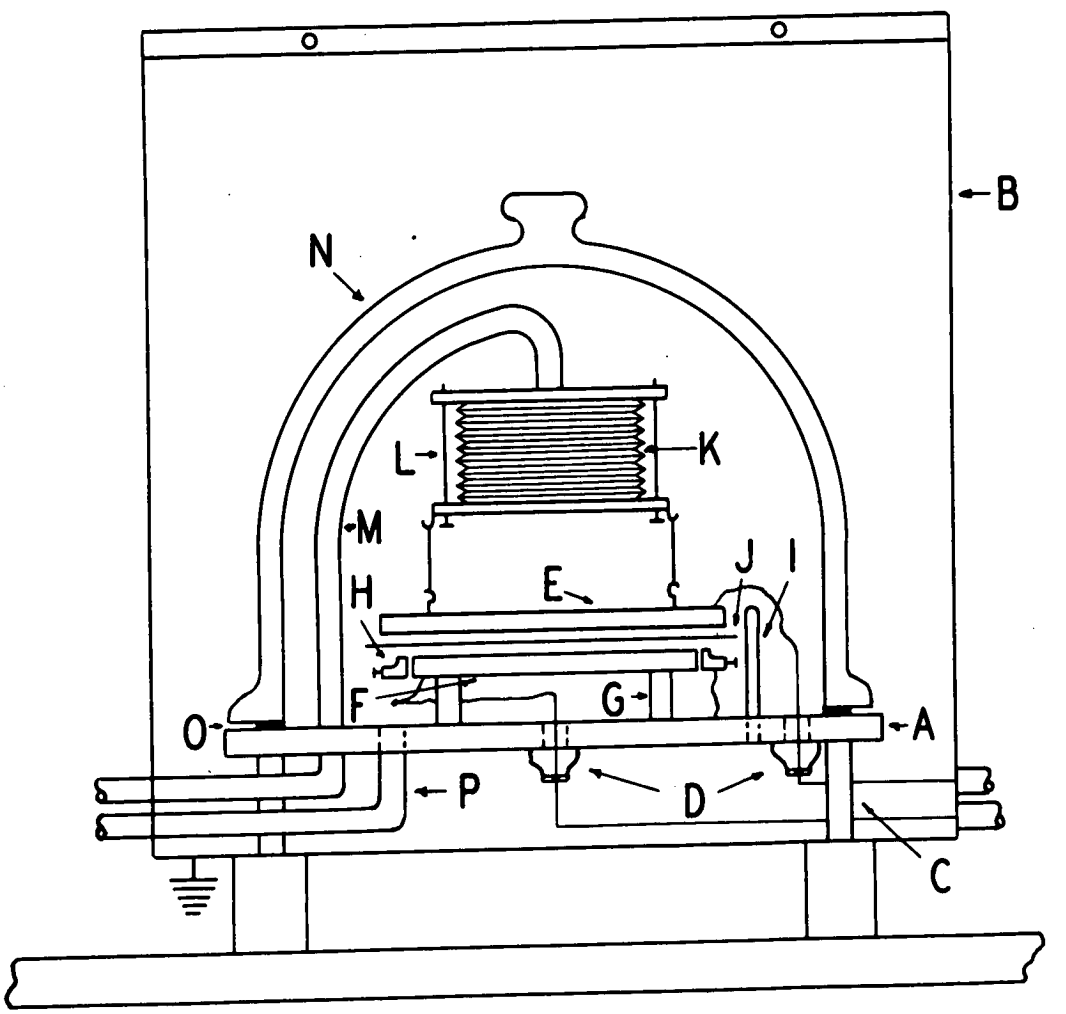

to metal seal. An electric current was passed through the loop to fuse the solder for attaching the loop to the lead-in wire. Connections were made from the loops to the upper electrode E and lower electrode F of the test capacitor, which was supported on glass pillars G to insulate it from the shield. The guard ring H is grounded directly to the base plate.

The copper finger I contains the cold junction of the thermocouple (see section on Heating the Test Chamber and Measurement of Temperature).

The top electrode E of the test capacitor is raised and lowered from the paper sample J by silk threads hooked to the metal bellows K. The top electrode is in a raised position when the sample is being dried and is lowered when electrical measurements are to be taken. The bellows is 1-1/8 inches long by 1-7/8 inches in diameter, and is closed at both ends by soldering the top and bottom to two brass plates. Four guide rods L with stop nuts at the ends limit the extension of the bellows to about 1/4 inch. The bellows is connected to the vacuum system by a copper tube M, which serves also as a mechanical support.

A bell cover N, resting on a rubber gasket O, encloses the test chamber. The test chamber is connected to the vacuum system through metal tubing P.

The top and one side of the shield box B are removable, so that the bell cover can be raised and a new sample slid into place.

GROUNDING THE SHIELD BOXES

The shield boxes for the various bridge units were interconnected by a web of wires, avoiding as much as possible the creation of inductive loops. The central point of the web was connected to a low resistance ground.

THE VACUUM SYSTEM

Vacuum is produced in the test chamber and bellows by the use of a Cenco Hyvac pump. The vacuum control system, mounted on the wooden support, is shown in Figure 14. The control system is connected to the vacuum pump by hose A, which leads to a trap to catch any oil that may be thrown back by the pump. Stopcock B and the Pirani gage C are in the vacuum line leading to the test chamber. The indicating meter for the Pirani gage is shown at J in Figure 3. In most cases, a pressure of less than 1 micron of mercury, as indicated by the Pirani gage, could be maintained in the test chamber. Stopcocks D and E and manometer F are used to control the bellows system. Stopcock E is connected to the nitrogen purifying system (see the section of Nitrogen Purifying System) by a rubber hose.

At the beginning of a test run, stopcock E is closed and stopcocks B and D opened. Thus, both the bellows and test chamber are evacuated, and the upper test electrode is in a raised position for drying the sample. In order to lower the upper test electrode to make a measurement and at the same time continually evacuate the test chamber, stopcock D is closed and E carefully opened to admit nitrogen from

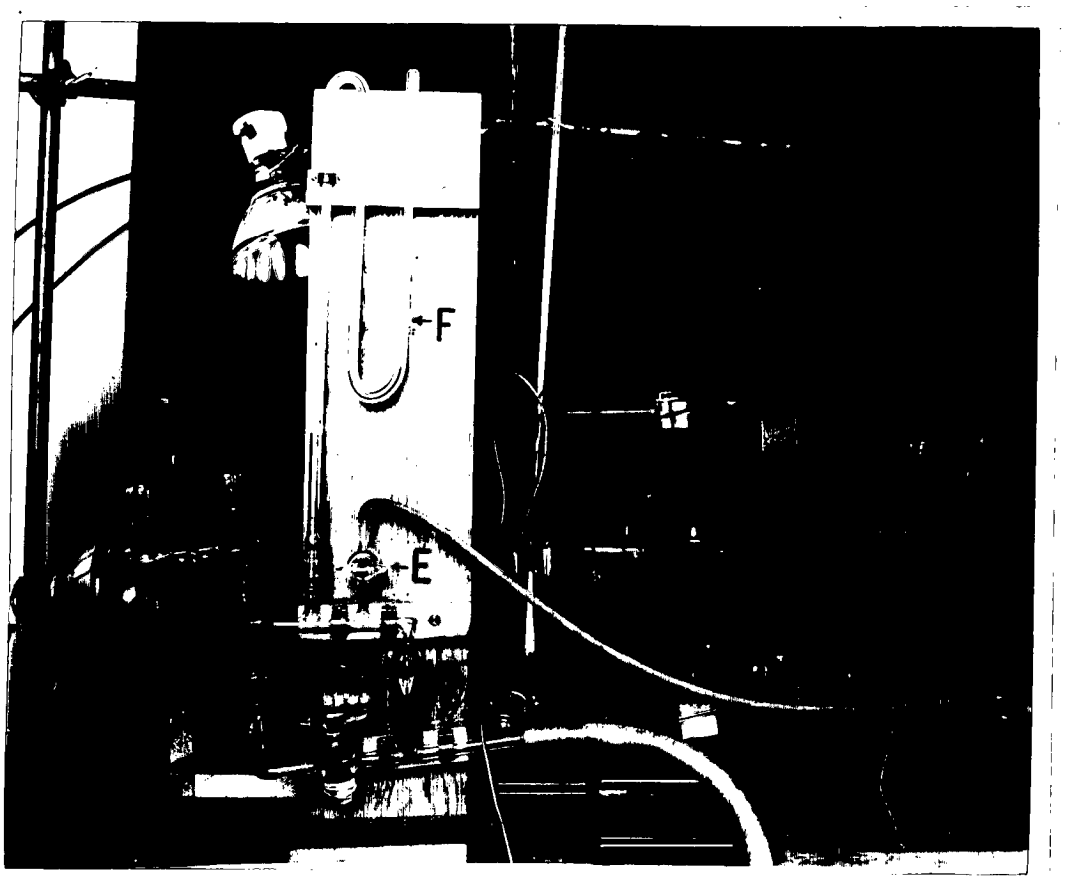

Figure 14

Vacuum Control System and Heating System
for the Test Chamber

the purifying system to the bellows. A few centimeters' pressure of nitrogen, as indicated by the manometer, is sufficient to extend the bellows. In order to raise the upper test electrode after a measurement and to continue drying the sample, the bellows is evacuated by closing stopcock B and opening D. After a minute or so, stopcock B is opened and pumping begins again on the test chamber.

Flushing the test chamber with nitrogen contained in the bellows can be accomplished by opening stopcock D without first closing B.

HEATING THE TEST CHAMBER AND MEASUREMENT OF TEMPERATURE

The shield I (Figures 3 and 14) containing the test chamber is heated by means of radiation from two 150-watt General Electric projector spotlights shown at G in Figure 14. To increase absorption of the radiation, one side and top of the shield box I were painted a dull black. With both spotlights close to the shield box and on full, a temperature of 70° C. could be maintained easily in the test chamber. Temperatures lower than 70° C. were obtained by rheostats in series with the spotlights.

The temperature inside the test chamber was measured by a chromel-alumel thermocouple system. The cold junction is contained in a copper finger soldered into the base of the test chamber and extending inside the test chamber close to the test capacitor (I, Figure 13). The hot junction is maintained at 100° C. on the boiling water bath H (Figure 14). The thermoelectric current is measured by a Weston

galvanometer 440 shown at J (Figure 14). To reduce the thermoelectric current to the range of the galvanometer, a 250-ohm resistor is used in series with the galvanometer.

Calibration data for the thermocouple are given in Table IV, and the calibration curve is plotted in Figure 15.

TABLE IV

CALIBRATION DATA FOR THE CHROMEL-ALUMEL THERMOCOUPLE

(Hot junction maintained at 100° C.)

Temperature ° C.	Meter Reading
23.7	5.7
33.0	9.5
45.5	15.0
57.5	20.0
72.0	26.0
82.5	30.5
93.0	35.0
101.0	38.5
110.0	43.0
120.0	47.0
130.5	51.0

NITROGEN PURIFYING SYSTEM

Nitrogen gas from the cylinder K (Figure 3) passes through the reducing valve L to the purifier M, which contains an electrically heated copper element to remove traces of oxygen. The purifier M is a

Figure 15

Calibration Chart for Chromel-Alumel Thermocouple

(Hot junction maintained at 100° C.)

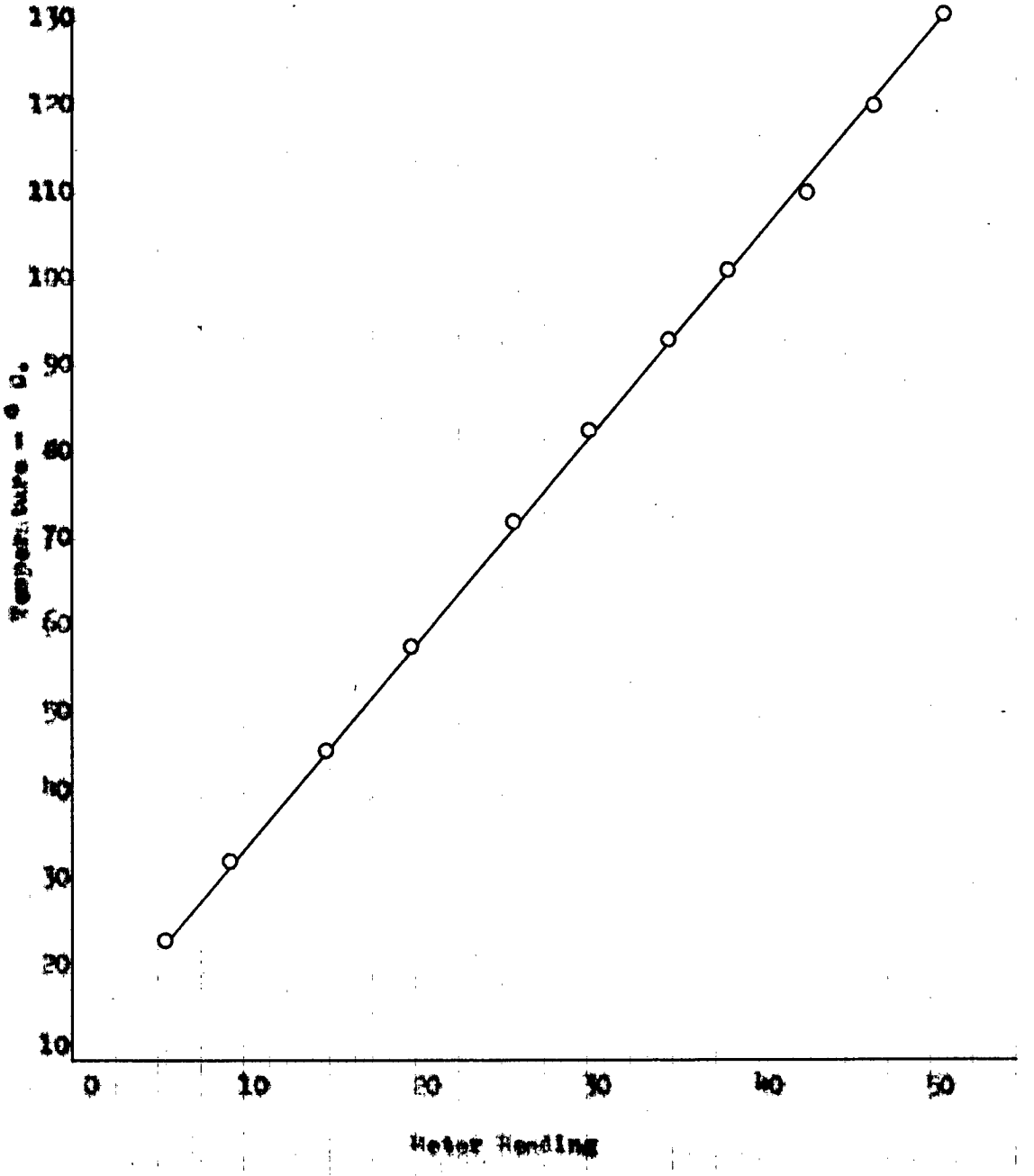

modified Kendall tube described by Savage and Ordal (29). The use of oxygen-free nitrogen for flushing the test chamber eliminated the possibility of oxidizing the test sample while flushing at elevated temperatures. Nitrogen leaving the purifier H passes through the trap M to protect the purifier in case oil should be sucked back from the oil bubbler O when the reducing valve L and the heating element of the purifier are turned off. The purified nitrogen is passed through drying tubes P filled in order with anhydrone, phosphorus pentoxide, and glass wool. The anhydrone accomplishes the preliminary drying and phosphorus pentoxide the final drying. Glass wool in the last tube serves as a dust catcher to remove particles of desiccant which may be mechanically carried by the gas stream. The gas leaving the last of the three tubes is drawn into the test chamber through the gas inlet E (Figure 14). The flow of nitrogen through the purifying apparatus is regulated by the reducing valve L (Figure 3) by observing the bubbler O when no gas is being drawn into the system; the bubbler bypasses the nitrogen to the atmosphere.

Phosphorus pentoxide is an efficient desiccant for use in the final drying. The partial pressure of water vapor leaving the purifier should be lower than 1.9×10^{-5} millimeters of mercury as calculated from data given in the International Critical Tables (30).

SEPARATION GAGE

In calculating the dielectric constant and loss angle, it is necessary to know the separation of the plates d at the center of the test capacitor when the sample is placed between the test electrodes.

To do this, the separation gage shown in Figure 16 was constructed.

A circular disk of plate glass A (Figure 16) equal in area to the test electrodes, a base plate B, and a lever C were cut from a piece of polished plate glass 5/16 inch thick. The glass disk and lever were carefully checked for flatness against the base plate and against an optical flat by observing interference patterns produced when the cleaned surfaces were placed together. The fulcrum edge D of the lever was ground square, and a millimeter scale was cemented to the sides of the lever. The lever is held firmly in position by a pivot E. A sensitive level F rests on one end at the center of the disk A, and other end pivots in a ground depression in the lever marking a known distance from the fulcrum. A rod H of known diameter slides between the lever and base plate. The base plate rests on a base board K provided with three leveling screws I.

To measure the separation d, all the glass parts are first carefully cleaned with a dean chamois leather to remove all grit and foreign particles and the instrument leveled by adjustment of screws I with a load on the disk equal to the total weight on the sample in the test capacitor. The sample is quickly removed from the test capacitor, placed beneath disk A, and the level returned to its initial position by adjustment of rod G. No difficulty was experienced because of hygro-expansive changes in the sample on transferring it from the dry conditions in the test chamber to the atmosphere, provided the measurement of d was completed before cockle developed. The development of cockle gives rise to erratic d values, which are sensitive to the loading on disk A.

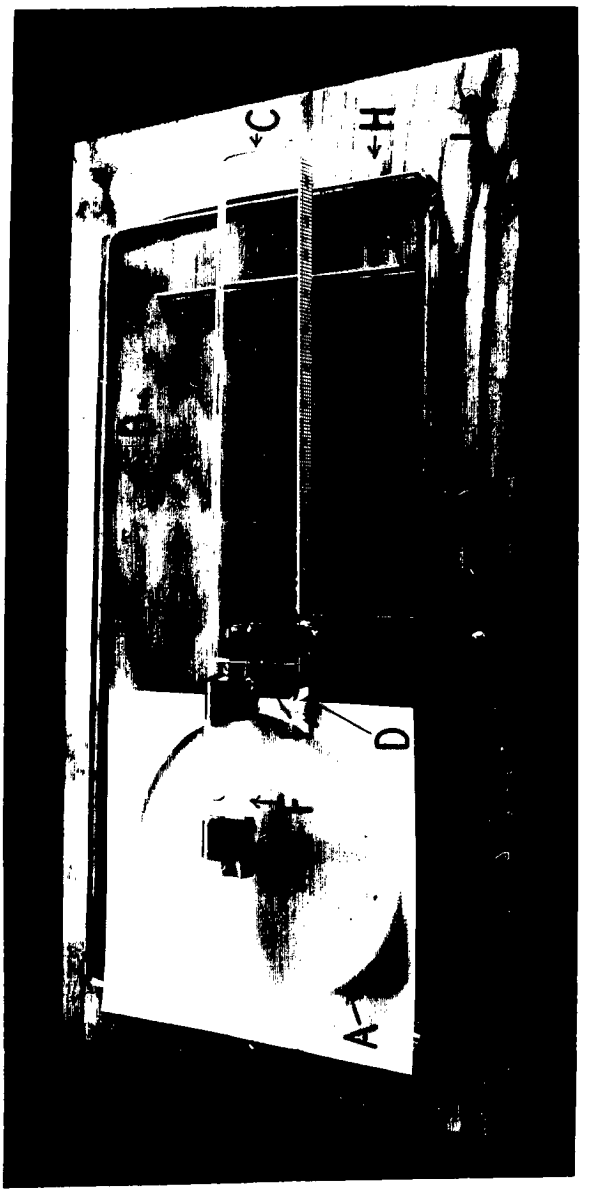

Figure 16

Separation Gage

The separation d is computed as follows:

$$d = \frac{\text{distance of level to fulcrum (1.10 cm.)}}{\text{distance of rod to fulcrum}} \times \text{diameter of rod}$$

The level F will indicate a deflection of 1 minute per scale division. Assuming adjustments of the level to a tenth of a division possible, the sensitivity S is

$$S = (1.10)/(10 \times 60 \times 57.3) = 3.2 \times 10^{-5} \text{ cm.}$$

THEORETICAL CONSIDERATIONS

THE EQUIVALENT ELECTRICAL CIRCUIT OF THE BRIDGE

The equivalent electrical circuit of the bridge is given in Figure 17. Because C_1, C_2, and C_p are not perfect capacitors free of dielectric loss, they are represented in Figure 17 by an ideal capacitance in parallel with a high resistance. C_p' represents the capacitance of the guard ring to the upper test electrode of the capacitor C_p. C_p' comes into play only when the test capacitor C_p is in the circuit. The equivalent parallel resistance of C_p' is large as compared with R_6, and hence its reciprocal is neglected.

In order to reduce the capacitance C_p' to a minimum, the effective guard ring area was reduced as described on page 37. Capacitors as large as 100 mmfds. were chosen for C_5 and C_6 in the Wagner ground to compensate for the added capacitance C_p'. This is an important point in the selection of suitable capacitors for the Wagner ground, and A.S.T.M. (1) is in error in stating that C_5 and C_6 need be two or three plate-type capacitors of such a range that their (opposite) extreme positions will cover any unbalanced or stray capacitances between the shields and the measuring circuit.

PROCEDURE FOR OBTAINING C_p AND δ OF THE TEST CAPACITOR

With the test capacitor C_p (Figure 2) out of the circuit by turning switch S_2 to the shield, the bridge is balanced by successive adjustments of C_2 and C_4, alternating with adjustments of the Wagner ground (the latter being with S_1 to ground). When the bridge detector

Figure 17

Equivalent Electrical Circuit of the Bridge

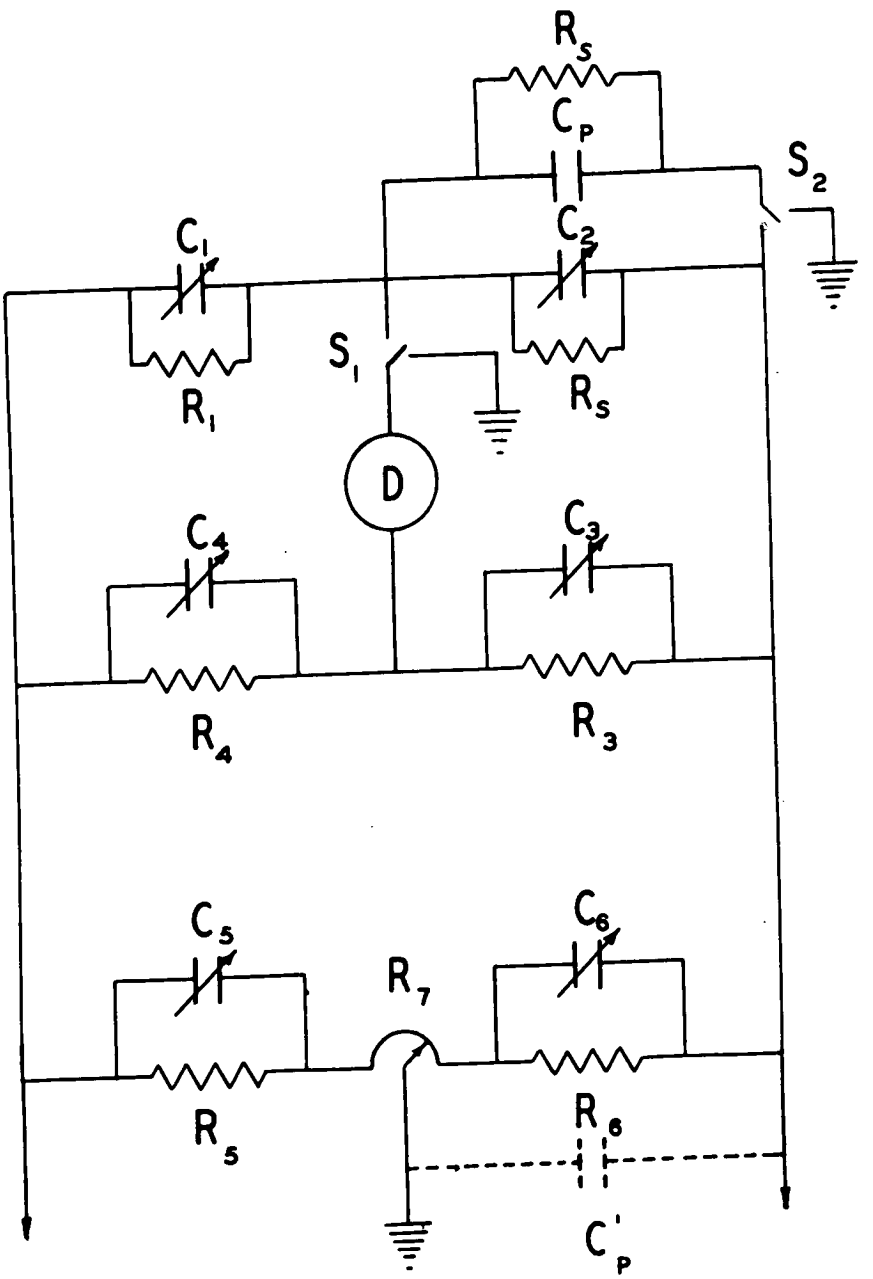

D shows complete balance with the switch S_1 in either position, the readings of C_2 and C_4 are recorded. With the switch S_2 turned so that the test capacitor C_p is in the circuit, new balance values of C_4 and C_2 are obtained. From the four values thus secured, the equivalent parallel capacitance and loss angle of the test capacitor are calculated from the following approximation formulas given by A.S.T.M. (1):

$$C_p = C_2 - C_2', \text{ and} \tag{1}$$

$$\delta^* = (C_2/C_p)\, 2\pi f R_4 (C_4' - C_4)/10^{12}, \tag{2}$$

where

C_p = the equivalent parallel capacitance of the test capacitor, in mmfds.,

C_2' = the capacitance of the variable air capacitor in parallel with the test capacitor when the latter is in the circuit, in mmfds.,

C_2 = the capacitance of the variable air capacitor when balance has been restored after the test capacitor has been disconnected from the circuit, in mmfds.,

C_4' = the capacitance of the capacitor C_4 when the test capacitor is in the circuit, in mmfds.,

C_4 = the capacitance of the capacitor C_4 when the test capacitor is out of the circuit, in mmfds., and

f = the frequency in cycles sec.$^{-1}$.

As f in all the present work was 1000 cycles sec.$^{-1}$, R_4 = 10,000 ohms, and as C_4 = Δ Dial Reading x 1.14 (see page 28), Equation 2 is used in the form

$$\delta = (C_2/C_p) \times 2\pi \times 10^{-5} \times \Delta \text{ Dial Reading} \times 1.14$$

$$= (C_2/C_p)\, \Delta \text{ Dial Reading} \times 7.16 \times 10^{-5}. \tag{3}$$

As C_2 and C_p can be measured to at least a precision of 1 part in 1000, the greatest source of error in the computation of δ

* A.S.T.M.'s notation $\tan \delta_p$ has been replaced by δ.

lies in the expression ($C_4' - C_4$). It was shown by a special experiment that values of δ were independent of the arbitrary C_2, and it is advantageous, therefore, to choose C_2 as small as possible to make ($C_4' - C_4$) as large as possible. In Equation 3, Δ Dial Reading was obtained by the difference of the means of ten readings of C_4' and C_4. In general, for dry paper samples Δ Dial Reading is of the order of 10 to 15 units with a probable error of $\pm$ 0.1 unit for C_4 and C_4'.

Errors Involved in the Use of the Approximation Formulas

A.S.T.M. (1) gives the following exact formulas for calculating $\tan \delta_p$ and C_p:

$$C_p = \frac{C_2 (1 + \tan \gamma_4 \tan \delta_2)}{1 + \tan \gamma_4' \tan (\delta_2 + \gamma_4' - \gamma_4)} - C_2', \text{ and} \qquad (4)$$

$$\tan \delta_p = (1 + C_2'/C_p) \tan (\delta_2 + \gamma_4' - \gamma_4) - C_2' \tan(\delta_2')/C_p), \qquad (5)$$

where

$\tan \delta_2' = 1/\omega C_2' R_s'$ = loss angle of C_2 at first setting.

$\tan \delta_2 = 1/\omega C_2 R_s$ = loss angle of C_2 at second setting.

$\tan \gamma_4 = \omega C_4 R_4$, and

$\tan \gamma_4' = \omega C_4' R_4$.

As previously stated, $R\omega C_2^2 = 0.04 \times 10^{-12}$ at 1000 cycles sec.$^{-1}$ for the capacitor C_2, where R is the equivalent series resistance. As $R\omega C_2^2$ is approximately constant with setting,

$$\tan \delta_2' = 1/\omega C_2' R_s' = R\omega C_2'^2/C_2' = 0.04 \times 10^{-12}/C_2'$$

and

$$\tan \delta_2 = 1/\omega C_2 R_s = R\omega C_2^2/C_2 = 0.04 \times 10^{-12}/C_2.$$

At 1000 cycles sec.$^{-1}$,

$$\tan \gamma_4 = \omega C_4 R_4 = 2\pi \times 1000 \times 10^{4} \times C_4 = 6.28\, C_4 \times 10^{7},$$

$$\tan \gamma_4' = \omega C_4' R = 2\pi \times 1000 \times 10^{4} \times C_4' = 6.28\, C_4' \times 10^{7}.$$

Assuming the usual values of 150.0 mmfds. for C_2', 500.0 mmfds. for C_2, 21.1 mmfds. for C_4', and 10.0 mmfds. for C_4, then at 1000 cycles sec.$^{-1}$ by the approximation formulas

$$C_p = 350.0 \text{ mmfds.}$$

$$\delta = 1.00 \times 10^{-3} \text{ radians,}$$

and by the exact formulas

$$C_p = [500.0\,(1 + 5.02 \times 10^{-8})/(1 + 1.06 \times 10^{-6})] - 150.0 = 350.0 \text{ mmfds.}$$

$$\tan \delta_p = [(1 + 150.0/350.0)\, 7.82 \times 10^{-4}] - [150.0 \times 2.7 \times 10^{-4}/350.0] = 1.11 \times 10^{-3} - 1.19 \times 10^{-4} = 1.00 \times 10^{-3},$$

where

$$\tan \gamma_4 = 6.28 \times 10^{-4},$$

$$\tan \gamma_4' = 13.3 \times 10^{-4},$$

$$\tan \gamma_2 = 0.30 \times 10^{-4}, \text{ and}$$

$$\tan \gamma_2' = 2.70 \times 10^{-4}.$$

The closeness of agreement of δ and $\tan \delta_p$ is rather surprising in view of the fact that $\tan \delta_2'$ and $\tan \delta_p$ are of the same order of magnitude. However, if the very good approximation $C_p = C_2 - C_2'$ is substituted in Equation 5, and also the approximation $\tan \theta = \theta$ for θ small, it is found that terms $1/R_s \omega C_2$ and $C_2'/R_s' \omega C_2 C_2'$ cancel, because the figure of merit $R\omega C^2$ for capacitor C_2 is approximately independent of setting. Hence, $\tan \delta_p$ is approximately independent of $\tan \delta_2$.

CALCULATION OF THE DIELECTRIC CONSTANT AND LOSS ANGLE OF A SAMPLE NOT COMPLETELY FILLING THE TEST CAPACITOR

In general, the test sample does not completely fill the test capacitor because of local high spots or zones in the sheet or because of cockle; therefore, the dielectric constant and loss angle of the incompletely filled test capacitor as calculated from bridge measurements will be essentially different from the actual dielectric constant and loss angle of the sample.

Let it be assumed that a parallel plate capacitor with a slab of dielectric whose thickness $\underline{t}$ is less than the separation of the plates $\underline{d}$ as shown in Figure 18.

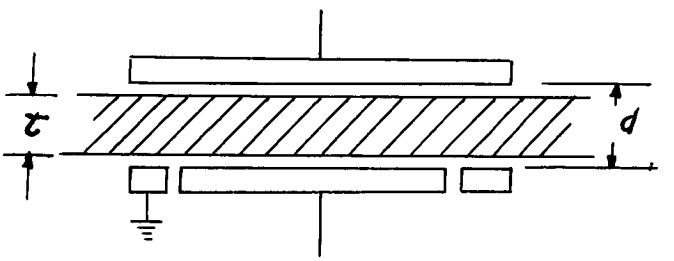

Figure 18

Actually, in practice the sample will not separate the electrodes quite parallel, but the correction is negligible for small angles of deviation from parallelism. The potential $\underline{V}$ between the plates is given by

$$\underline{V} = 4\pi\sigma\underline{t}/\underline{K}' + 4\pi\sigma(\underline{d} - \underline{t}), \qquad (6)$$

where $\underline{K}'$ is the dielectric constant of the slab, and σ is the charge density per unit area on the electrodes, As

$$\sigma = \underline{C}_p \underline{V}/\underline{A}, \qquad (7)$$

where $\underline{A}$ is the area of the lower test electrode and $\underline{C}_p$ is the capacitance of the incompletely filled capacitor. Combining equations 6 and 7,

$$C_p = \frac{A}{4\pi[d - t(K' - 1)/K']} \text{ in e.s.u.} \qquad (8)$$

Knowing C_p, A, d, and t by direct measurement, the dielectric constant K' of the slab can be computed.

The loss angle of the incompletely filled test capacitor is measured by the bridge. The question arises, what is the loss angle of the slab? This can be answered by considering the capacitor shown in Figure 19, of capacitance C_p', completely filled with a dielectric of thickness t and dielectric constant K'.

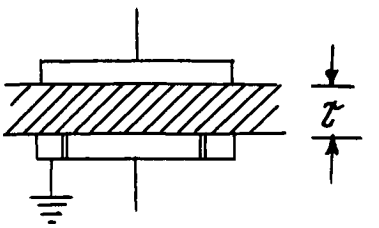

Figure 19

The power dissipated by a capacitor is given by

$$P = V^2/R \qquad (9)$$

for small loss angles, where V is the potential between the plates and R is the equivalent parallel resistance. The power dissipated by the capacitors shown in Figures 18 and 19 will be the same if the field strength in the dielectric slab is the same. Or

$$(V'/V)^2 = R'/R, \text{ if } E = E' = 4\pi C_p V/K' A = 4\pi C_p' V'/K' A, \qquad (10)$$

where

V' = the potential between the electrodes (Figure 19),

R' = the equivalent parallel resistance (Figure 19),

C_p' = the capacitance (Figure 19),

$E = E'$ = the field strength in the dielectric slab,

V = the potential between the electrodes (Figure 18)

$\underline{R}$ = the equivalent parallel resistance (Figure 18),

$\underline{C}_p$ = the capacitance (Figure 18),

$\underline{A}$ = the area of the lower test electrode, and

$\underline{K}'$ = the dielectric constant of the slab.

The loss angle δ' of Figure 19 is given by

$$\delta' = 1/\ \underline{C}_p'\ \underline{R}' = (1/\omega\ \underline{C}_p\ \underline{R})\ (\underline{R}/\underline{R}')\ (\underline{C}_p/\underline{C}_p')$$
$$= \delta(\underline{V}/\underline{V}')^2\ (\underline{V}'/\underline{V}) = \delta(\underline{V}/\underline{V}') = \delta(\underline{C}_p'/\underline{C}_p). \qquad (11)$$

As $\underline{C}_p$ is given by Equation 8, and $\underline{C}_p'$ is given by $\underline{K}'\ \underline{A}/4\ \pi\underline{t}$, Equation 11 takes the final form

$$\delta' = \delta[1 + \underline{K}'\ (\underline{d} - \underline{t})/\underline{t}]. \qquad (12)$$

ERRORS RESULTING FROM DIELECTRIC LOSSES IN THE TEST CAPACITOR AND LEADS

The equivalent circuit of the test capacitor showing dielectric loss, in addition to that resulting from the sample, is shown in Figure 20.

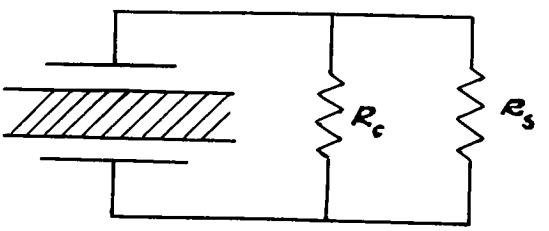

Figure 20

The loss angle δ for the combination shown in Figure 20 is given by

$$\delta = (\underline{R}_s + \underline{R}_c)/\underline{R}_s\ \underline{R}_c\ \underline{C}\omega. \qquad (13)$$

where

R_s = the equivalent parallel resistance of the sample,

R_c = the equivalent parallel resistance of the test capacitor, and

C = the capacity of the test capacitor.

The loss angle δ_s of the sample alone is

$$\delta_s = 1/R_s C \omega. \tag{14}$$

Then, by combining Equations 13 and 14,

$$\delta_s = [1/(1 + R_s/R_c)]. \tag{15}$$

The correction factor $1/(1 + R_s/R_c)$ was determined over a range of relative humidities and temperatures as a part of the determination of the loss angle-temperature hysteresis loops (see the section on Experimental Data and Discussion). The loss angle of the test capacitor δ was measured with the upper electrode in the raised position with the sample in place. Any contribution to δ by the sample when measured with the upper electrode raised will certainly be small, as the ratio $(d - t)/t$ becomes very large (see Equation 12).

The loss angle δ_s for the average sample at a capacitance of 350 mmfds. is approximately

$$\delta_s = 1.0 \times 10^{-3} = 1/R_s C \omega,$$

or

$$R_s = 4.5 \times 10^8 \text{ ohms.}$$

The loss angle δ_c for the test capacitor at a capacitance of 50 mmfds. was found to be independent of relative humidity and temperature over the range tested, and is approximately

$$\delta_c = 1.6 \times 10^{-4} = 1/\underline{R}_c \underline{C}\omega,$$

or

$$\underline{R}_c = 2.0 \times 10^{10} \text{ ohms.}$$

Then in equation 15, $\underline{R}_s/\underline{R}_c = 2.3 \times 10^{-2}$, which is about 2 per cent; therefore, the correction factor may be disregarded and δ_s may be considered equal to δ within the limits of experimental error.

EXPERIMENTAL PROCEDURES

PREPARATION OF TEST SHEETS

All test sheets used in this thesis were prepared from Brown Company unbleached kraft sold under the name of "special washed sulphate," which is a pulp specially prepared for the manufacture of condenser tissue. Test sheets were prepared over a wide range of densities, by varying the method of sheet making and wet pressing, to study the effect of sheet density on the dielectric constant K' and the loss factor $K'\delta'$. Special attention was paid to the production of uniform test sheets of good formation so as to reduce cockle problems to a minimum when the sheet was dried under the high vacuum conditions in the test chamber. Test sheets were prepared by three methods.

Method I

Unbleached kraft (Brown Company) was refined for 40 minutes in the Lemsén mill to a freeness of 750 cc. S.-R. (840 cc. S.-R. freeness for the unrefined pulp). Sheets were formed on the British sheet mold 1.4 grams in weight instead of the customary 1.2 grams and couched from the wire onto a filter paper. A second filter paper backed by a British disk was laid over the sheet and the combination pressed between blotters at 10 p.s.i. for 5 minutes. Duplicate sheets were given a second pressing at intervals of 10 p.s.i., 50 p.s.i., 350 p.s.i., and 5000 p.s.i. for 5 minutes with a change of blotters. Pressures of 350 p.s.i. and 5000 p.s.i. were obtained with an Elmes press. The finished sheets, together with the filter papers, were air dried on the British rings and stored on the rings over anhydrone in a

desiccator until ready for use. Sheets formed by Method I are of matt finish and low in density.

Method II

Unbleached kraft (Brown Company) was refined for 40 minutes in the Lampén mill as in Method I. Sheets were formed on the British sheet mold 1.0 gram in weight instead of the customary 1.2 grams and couched from the wire onto a filter paper. A British disk was laid over the sheet and the combination pressed between blotters at 10 p.s.i. for 5 minutes. For the smoothing press the blotters and filter paper were removed, a smooth square of moistureproof cellophane placed on the sheet, and a second British disk laid on the cellophane. Duplicate sheets were given a smoothing press with the sheet-cellophane combination between blotters at intervals of 10 p.s.i., 50 p.s.i., 350 p.s.i., and 5000 p.s.i. for 5 minutes. The cellophane and upper disk were removed, and the sheets were air dried on the British rings and then stored on the rings over anhydrone in a desiccator until ready for use. Sheets formed by Method II have a smooth finish and intermediate density.

Method III

Unbleached kraft (Brown Company) was refined for 40 minutes in the Lampén mill as in Method I. Sheets were formed in the British sheet mold 1.0 gram in weight as in Method II. The formed sheets were couched onto a blotter, a British disk laid over the sheet, and the combination pressed at 10 p.s.i. for 5 minutes. After pressing, the blotter was carefully removed and the first sheet on the disk registered with a second sheet on a blotter prepared in the same way; the two

were laminated at 10 p.s.i. for 2 minutes, forming a two-ply sheet. The procedure was repeated to form a three-ply sheet. The three-ply sheet on the disk was given an additional pressing against a dry blotter at 10 p.s.i. for 2 minutes to remove as much water as possible. Duplicate sheets were given the final smoothing press against the cellophane and disk as outlined in Method II at intervals of 10 p.s.i., 50 p.s.i., 350 p.s.i., and 5000 p.s.i. for 5 minutes. The finished sheets were air dried on the British rings and stored on the rings over anhydrone in a desiccator until ready for use. Sheets formed by Method III have a smooth finish and high density.

TESTING THE SHEETS AND CALCULATION OF THE DIELECTRIC CONSTANT K' AND LOSS ANGLE δ

When the sheets were ready for use, they were removed from the rings in the desiccator (at about 1.4 per cent moisture content), cut to 3-3/4 by 3-3/4 inches and visually inspected by transmitted light for local high spots and imperfections. Any surface irregularities were carefully erased by means of a sharp razor blade. The inspected sheets were quickly transferred to the test chamber and the sample dried under vacuum with the upper test electrode in the raised position at 70° C., unless otherwise noted.

Bridge Measurements

The necessary bridge measurements required for the computation of C_p and were made according to the procedure outlined on page 52.

Measurement of the Electrode Separation

The electrode separation d was determined using the separation gage and procedure described on page 48.

Measurement of the Sample Thickness

The sample thickness t was measured at the conclusion of the run, using the standard Schopper caliper over the entire area of the sheet included between the electrodes. The mean value of t was used in the computations.

Measurement of the Sample Density

The density of the sample is defined as the oven-dry weight of the sample included between the effective area of the test electrodes divided by the volume of the sample between the effective area of the test electrodes. Or, the density in gm. cm.$^{-3}$ is given by

$$\rho = W / A\,t, \qquad (16)$$

where

W = the oven-dry weight of the sample included between the the effective area of the electrodes, in grams,

A = the effective area of the electrodes = the area of the lower electrode plus one half the area of the guard ring clearance, in sq. cm. = 45.63 sq. cm., and

t = the Schopper caliper of the sheet in cm.

Calculation of the Corrected Dielectric Constant K'

Equation 1 was used for calculating C_p from bridge measurements. For the calculation of the corrected dielectric constant K', Equation 8 in practical units becomes

$$C_p = \frac{1.11\ A}{4\pi\,[d - t(K' - 1)/K']}. \qquad (17)$$

where

C_p = the equivalent parallel capacitance of the test capacitor, in mmfd. as computed from Equation 1.,

A = the effective area of the test electrodes = the area of the lower test electrode plus one half the area of the guard ring clearance, in sq. cm. = 45.63 sq. cm.,

d = the separation of the electrodes, in cm.,

t = the thickness of the sample, in cm., and

K' = the corrected dielectric constant.

Calculation of the Corrected Loss Angle δ'

Equation 3 was used to calculate the loss angle δ. For the calculation of the corrected loss angle δ', Equation 12 was employed.

EXPERIMENTAL DATA AND DISCUSSION

FLUSHING AS AN AID TO DRYING

It is an established fact that the loss angle and dielectric constant of paper decrease as the moisture content decreases. Data covering the effect of drying with and without flushing on the loss angle δ and capacitance C_p of the test capacitor at 1000 cycles $sec.^{-1}$ by evacuating to 1-2 microns of mercury at 70° C. are given in Table V and plotted in Figure 21. In the flushing curve of Figure 21, the test chamber was swept out with dry oxygen-free nitrogen every half hour for the first 4 hours of pumping. Two sheets prepared by Method I and pressed at 50 p.s.i. were used in this experiment.

It is to be noticed that the flushing technique is effective to the extent that equilibrium was attained in about 4 hours, whereas for a sample prepared in the same way, pumping without flushing required about 5 hours to attain equilibrium. Apparently, flushing is effective in any system from which vapors and gases different from the flushing gas are to be removed in an arrangement where there are at least two flow resistances in series such as an enclosure within an enclosure with small openings between them. This condition would certainly obtain in the porous structure of paper.

One would expect flushing to be more effective in an absolutely airtight apparatus than in an apparatus with a minute leak. For example, if a sample is dried in an absolutely airtight chamber and the pump will sustain a pressure of 1 micron of mercury in the chamber, then at equilibrium the total pressure of 1 micron in the

TABLE V

δ AND C_p AT 1000 CYCLES SEC.$^{-1}$ AND 70° C.
VS. PUMPING TIME WITH AND WITHOUT FLUSHING

(50 psi. Pressing - Sheet Method I)

Sample	Pumping Time hours	C_p mmfds.	$\delta \times 10^3$ radians
50a	0.5	357.7	1.99
Flushing	1.0	356.9	1.61
	1.75	357.5	1.25
	2.25	357.7	1.05
	3.0	358.8	0.99
	3.5	359.3	0.92
	18.0	359.6	0.89
50b	1.0	395.4	2.00
No flushing	2.0	395.6	1.41
	4.0	401.2	1.04
	12.0	401.0	0.83
	17.0	400.7	0.80

chamber will eventually be due to water vapor. Now, let it be assumed that a sample is being dried in a chamber with a minute leak and that the pump will sustain a pressure of 1 micron of mercury. Then at equilibrium the partial pressure of water vapor will not exceed about 0.03 micron of mercury, because the ratio of the partial pressures of moisture and air swept in will be independent of the pressure. In the light of this picture, one would expect a much more rapid attainment of equilibrium using the flushing technique if the apparatus were perfectly airtight.

Figure 21

δ and η_p at 1000 Cycles Sec.$^{-1}$ and 70° C. vs. Pumping Time with and without Flushing

(50 pst. Pressing - Sheet Method I)

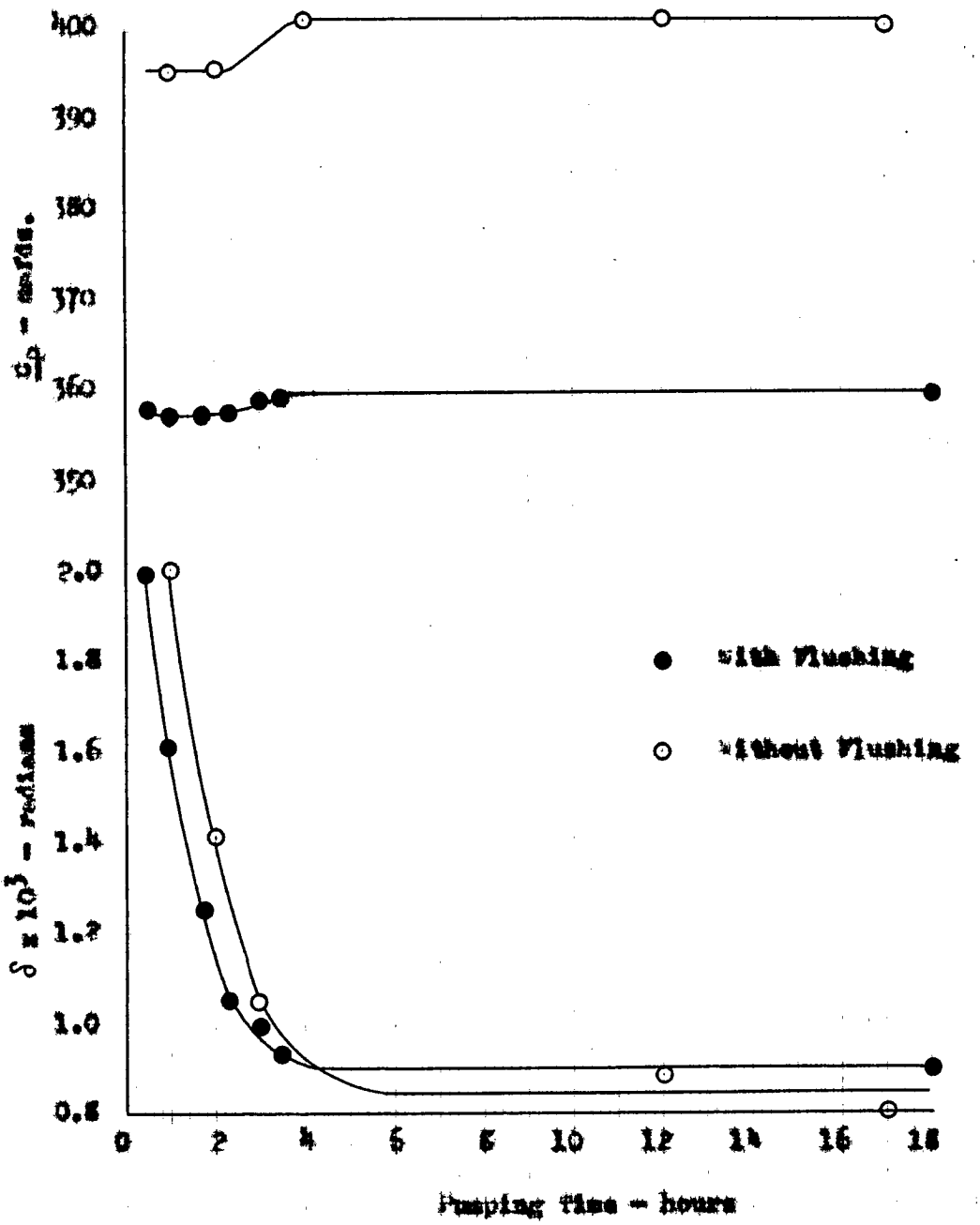

It will be noticed in the capacitance curves plotted in Figure 21 that a marked rise in capacitance occurs as the equilibrium value of δ is approached. This rise in capacitance was typical of many such curves determined during the course of this investigation. The sharp rise can be attributed to an increase in the dielectric constant of the sheet or to a decrease in the electrode separation $\underline{d}$ at this point as a result of hygroexpansive changes in the sheet. It is unfortunate that data are not available on this point.

DATA ON THE RELATION OF DIELECTRIC CONSTANT TO DENSITY

Data for the expression $(\underline{K}' - 1)/(\underline{K}' + 2)$ at 1000 cycles $sec.^{-1}$ and 70° C. are presented in Table VI and plotted in Figure 22. The advantage of establishing a functional relationship between the dielectric constant and the density would lie in the conversion of the dielectric constant of a given sheet to some standard density for purposes of comparison. This observation holds, likewise, for the loss angle.

In the absence of greater information, the curve of Figure 22 is represented as a straight line intersecting the density axis at 0.3 $gm.\ cm.^{-3}$. The classical Clausius-Mosotti relationship, stating that the expression $(\underline{K} - 1)/(\underline{K} + 2)$ is directly proportional to density, would be a straight line passing through the origin as represented by the dotted line in Figure 22.

In the computation of $\underline{K}'$, values of $\underline{C}_p$, $\underline{d}$, and $\underline{t}$ are required (see Equation 17). Of these values, $\underline{C}_p$ can be obtained to a precision of at least 1 part in 1000; however, the technique of

TABLE VI

DATA FOR THE CALCULATION OF THE $(K' - 1)/(K' + 2)$ EXPRESSION AT 1000 CYCLES SEC.$^{-1}$ AND 70° C. FOR VARIOUS DENSITIES

Sheet Method	Pressing p.s.i.	C_p mmfds.	$\underline{d}$ cm.	$\underline{t}$ cm.	K'	$\frac{(K' - 1)}{(K' + 2)}$	Density gm. cm.$^{-3}$
I	10a	354.0	0.0161	0.0127	1.59	0.164	0.62
	10b	566.8	0.0111	0.0084	1.95	0.240	0.70
	50a	332.0	0.0169	0.0142	1.50	0.143	0.64
	50b	374.9	0.0163	0.0118	1.88	0.230	0.66
	50c	597.3	0.0107	0.0086	1.84	0.219	0.66
	5000a	582.4	0.0106	0.0084	1.78	0.206	0.72
	5000b	386.0	0.0149	0.0107	1.70	0.189	0.72
II	10a	552.7	0.0102	0.0086	1.50	0.143	0.62
	10b	548.1	0.0112	0.0089	1.76	0.202	0.61
	50a	649.1	0.0094	0.0084	1.61	0.169	0.65
	50b	663.7	0.0092	0.0079	1.68	0.185	0.69
	350a	705.6	0.0092	0.0071	1.93	0.236	0.77
	350b	629.3	0.0105	0.0076	2.15	0.277	0.73
	5000a	676.4	0.0100	0.0074	2.20	0.286	0.71
	5000b	464.1	0.0109	0.0081	1.87	0.225	0.69
III	10a	267.0	0.0253	0.0204	1.82	0.215	0.74
	10b	310.2	0.0234	0.0204	2.04	0.257	0.79
	50a	306.5	0.0240	0.0191	2.20	0.286	0.83
	350a	326.6	0.0234	0.0186	2.46	0.328	0.87
	5000a	319.1	0.0223	0.0178	2.20	0.286	0.94
	5000b	314.2	0.0246	0.0198	2.48	0.330	0.84

measuring $\underline{d}$ and $\underline{t}$ is open to some question and might explain the departure from the Clausius-Mosotti function. Undoubtedly, measurement of $\underline{d}$ *in situ* without the necessity of transferring the sample to some external measuring device would be the best technique, and Mr. Paul Hansen, who is continuing this investigation as a Doctor's thesis at The Institute of Paper Chemistry, will devise some method for doing this. Furthermore, the thickness $\underline{t}$ was determined by the Schopper caliper with approximately 7.5 p.s.i. on the anvil. The thickness $\underline{t}$ of a sheet of paper is a difficult thing to define in work of this

Figure 22

$(K' - 1)/(K' + 2)$ at 1000 Cycles $Sec.^{-1}$ and 70^{0} C. vs. Density

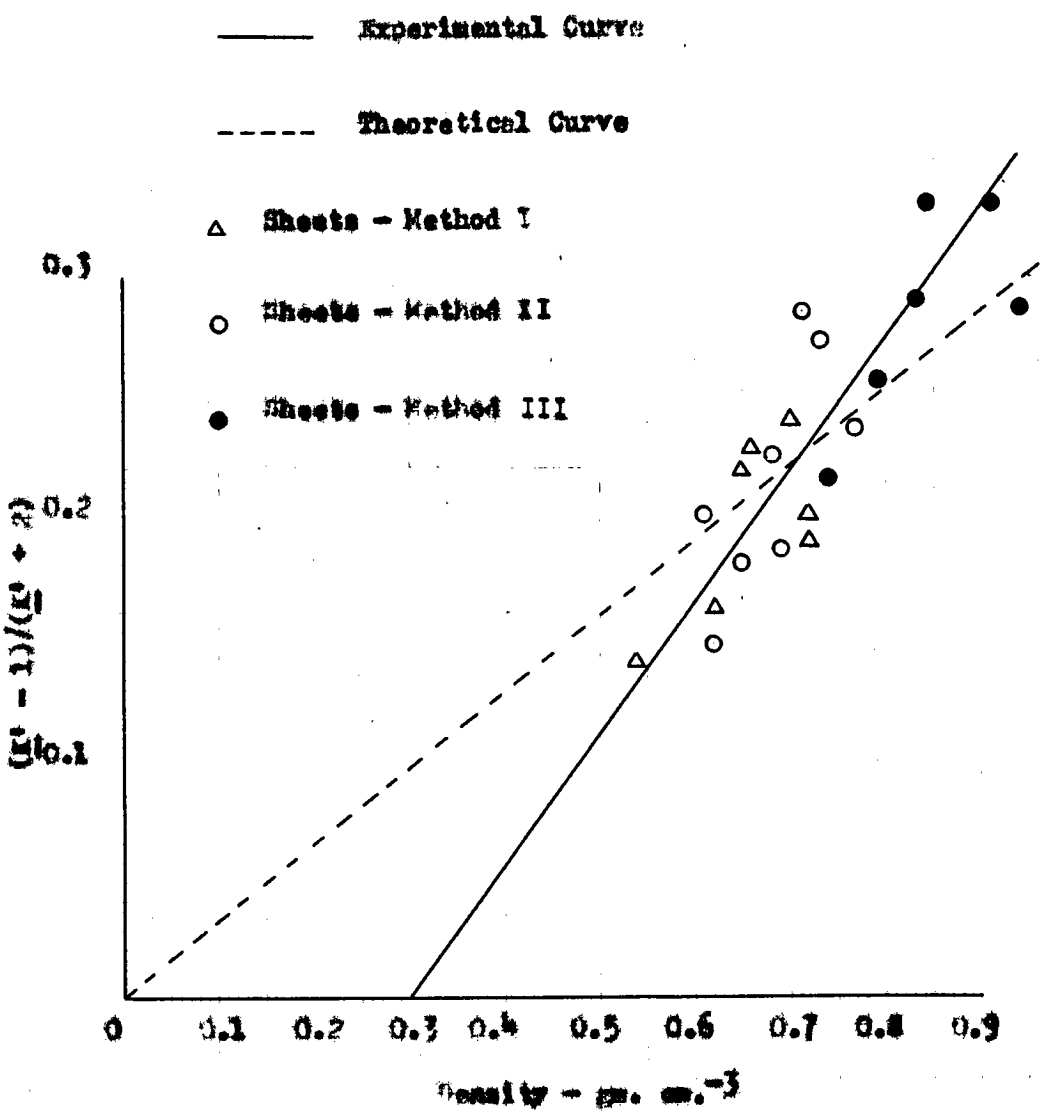

sort, and data on the compressibility would, therefore, be of interest. Low values of t would tend to increase the calculated density and increase K', other factors being equal.

DATA ON THE LOSS FACTOR $K'\delta'$ AS RELATED TO DENSITY

It has been stated that the power loss per unit volume of a dielectric at a stated frequency, voltage gradient, and temperature is proportional to the loss factor. Assuming that the power loss in a capacitor is proportional to the mass of material between the electrodes and to the square of the field strength, it is found that

$$P = V\,I\,\delta = (V^2 \omega \delta'\, K'\, A)/(4\pi t) \propto \rho\, A\, t\, (V/t)^2,$$

or

$$K'\delta' \propto P\rho/f, \tag{13}$$

where

δ' = the loss angle of the sheet,

K' = the dielectric constant of the sheet,

ρ = the density of the sheet, and

f = the frequency.

Thus, according to Equation 13, the loss factor $K'\delta'$ should be proportional to the density at a given frequency. Data for the loss angle $K'\delta'$ as related to density are given in Table VII and plotted in Figure 23. In the absence of greater information, the experimental curve of Figure 23 is represented as a straight line intersecting the density axis at 0.45 gm. cm.$^{-3}$. The ideal curve of loss factor versus density at a given frequency and temperature would be a straight line passing through the origin according to Equation 13.

TABLE VII

DATA FOR THE CALCULATION OF THE LOSS FACTOR $\delta' K'$ AT 1000 CYCLES SEC.$^{-1}$ AND 70° C. FOR VARIOUS DENSITIES

Sheet Method	Pressing p.s.i.	$\underline{d}$ cm.	$\underline{t}$ cm.	K'	$\delta \times 10^3$ radians	$\delta' \times 10^3$ radians	$\delta' K' \times 10^3$	Density gm. cm.$^{-3}$
I	10a	0.0161	0.0127	1.59	0.94	1.34	2.13	0.62
	10b	0.0111	0.0084	1.95	-	-	-	0.70
	50a	0.0169	0.0142	1.50	0.62	0.81	1.22	0.54
	50b	0.0163	0.0118	1.38	0.81	1.04	1.95	0.66
	50c	0.0107	0.0086	1.34	1.09	1.58	2.90	0.66
	5000a	0.0106	0.0084	1.78	1.10	1.61	2.86	0.72
	5000b	0.0149	0.0107	1.70	0.63	1.05	1.78	0.72
II	10a	0.0102	0.0086	1.50	0.83	1.14	1.71	0.62
	10b	0.0112	0.0089	1.76	0.91	1.32	2.32	0.61
	50a	0.0094	0.0084	1.61	0.96	1.09	1.76	0.65
	50b	0.0092	0.0079	1.68	0.92	1.13	2.30	0.69
	350a	0.0092	0.0071	1.93	0.86	1.35	2.61	0.77
	350b	0.0105	0.0076	2.15	0.85	1.56	3.34	0.73
	5000a	0.0100	0.0074	2.20	0.81	1.44	3.17	0.71
	5000b	0.0109	0.0081	1.87	0.89	1.26	2.36	0.69
III	10a	0.0253	0.0224	1.32	1.24	1.54	2.80	0.74
	10b	0.0234	0.0204	2.04	1.48	1.92	2.34	0.79
	50a	0.0240	0.0191	2.20	1.06	1.66	3.66	0.83
	350a	0.0234	0.0186	2.46	1.17	1.91	4.70	0.87
	5000a	0.0223	0.0178	2.20	1.15	1.80	3.96	0.94
	5000b	0.0246	0.0193	2.04	1.09	1.69	4.12	0.84

It was believed that the departure of the experimental curve of Figure 22 from the Clausius-Mosotti relationship might be responsible for the discrepancy noted in Figure 23. In conference with Dr. J. A. Van den Akker of The Institute of Paper Chemistry, it was learned that fibrous materials similar in nature to paper had been found to adhere rigorously to the Clausius-Mosotti relationship over a wide range of densities. With this in mind, the data of Table VII were recalculated on the assumption that C_p, $\underline{t}$, and density were not in error, but that errors in $\underline{d}$ were responsible for the departure from the Clausius-Mosotti

Figure 23

Loss Factor at 1000 Cycles Sec.$^{-1}$ and 10^{10} C. G. S. $\delta^1 g^1$ vs. Density

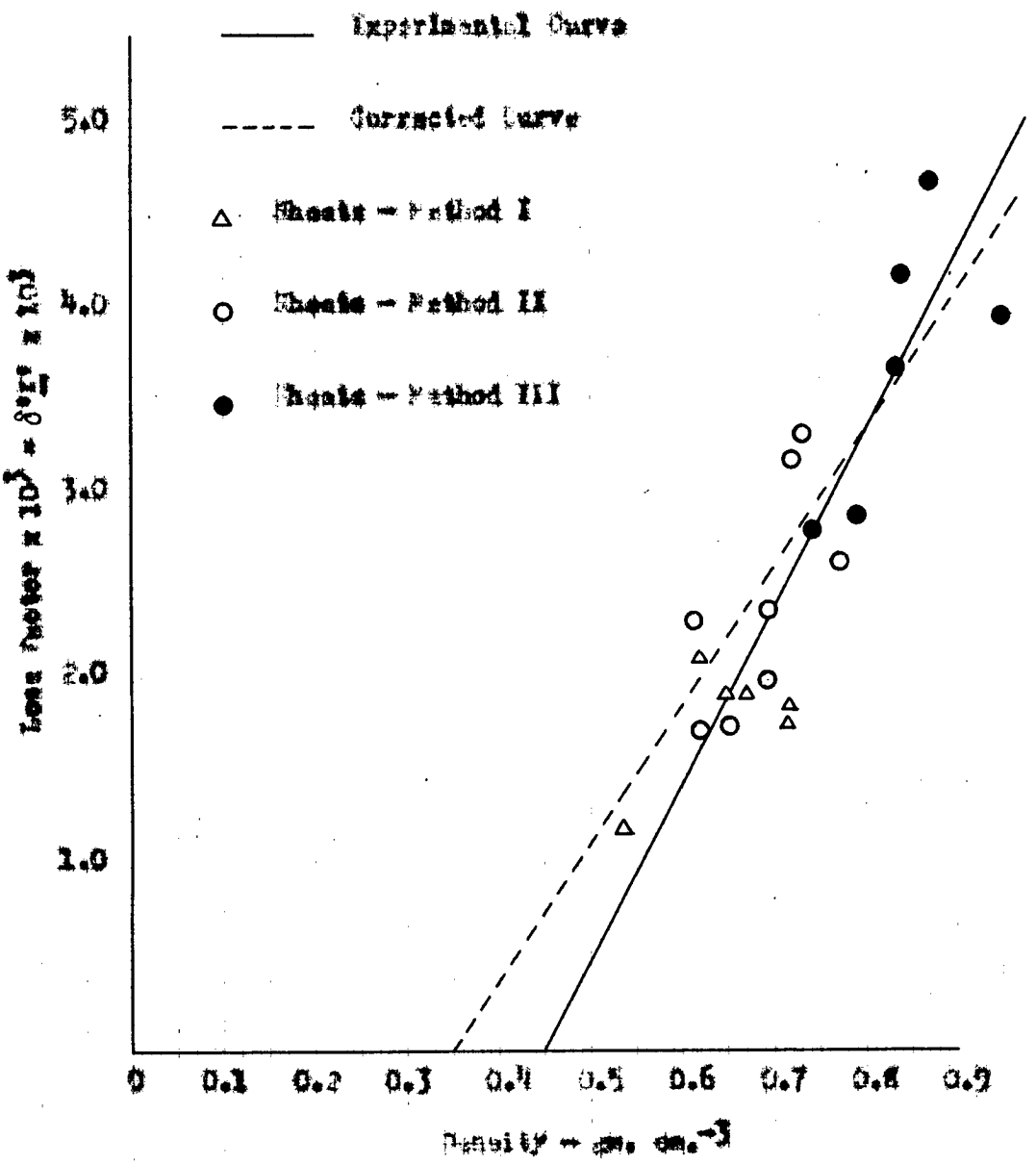

relationship. For a sheet of given density, an ideal dielectric constant K'' was calculated at that density from the dotted curve in Figure 22. Knowing C_p and t for the given sheet, a new value of d was calculated employing Equation 17. Using the new value of d and K'', δ'' was calculated by Equation 12. Data on the corrected loss factor $K''\delta''$, as related to density at 1000 cycles sec.$^{-1}$ and 70° C., are given in Table VIII and plotted in Figure 24. The corrected curve is represented as a dotted line in Figure 23 for purposes of comparison with the experimental curve.

It will be noticed in Figure 24 that the spread of points is somewhat less than in Figure 23, but errors in d alone responsible for the departure from the Clausius-Mosotti relationship do not explain the fact that the corrected curve in Figure 24 does not pass through the origin at zero density. This leads one to suspect strongly the values of t. At the lower densities, values of t would be too small as a result of the compressibility of the sheet. Then, for a given low density point, density decreases and both K'' and δ'' decrease as t is increased; the abscissa of low-density points in Figures 22, 23, and 24 would shift to the left, and ordinates of low density points in Figures 22, 23, and 24 would shift down. It might be possible that a corrected t value would give curves of smaller slope than in Figures 22, 23, and 24 and would pass through the origin.

LOSS ANGLE-TIME RELATION HYSTERESIS LOOPS

During the course of this investigation it was noticed that, when a sample had reached its equilibrium value of δ at 70° C. and if

TABLE VIII

DATA FOR THE CALCULATION OF CORRECTED LOSS FACTOR
$\delta''\underline{K}''$ AT 1000 CYCLES SEC.$^{-1}$ AND 70° C.

Sheet Method	Pressing p.s.i.	$\underline{d}$ cm.	$\underline{t}$ cm.	$\underline{C}_o$ mmfds.	$\underline{K}''$	$\delta \times 10^3$ radians	$\delta'' \times 10^3$ radians	$\underline{K}''\delta'' \times 10^3$	Density γ_3 gm. cm.^{3}
I	10a	0.0167	0.0127	254.0	1.72	0.94	1.45	2.50	0.62
	10b	–	–	–	–	–	–	–	–
	50a	0.0178	0.0142	332.0	1.60	0.62	0.88	1.40	0.54
	50b	0.0158	0.0118	374.9	1.80	0.61	0.98	1.77	0.66
	50c	0.0105	0.0086	507.3	1.80	1.09	1.53	2.75	0.66
	5000a	0.0108	0.0084	582.4	1.88	1.10	1.66	3.12	0.72
	5000b	0.0154	0.0107	386.0	1.83	0.63	1.15	2.15	0.72
II	10a	0.0109	0.0086	552.7	1.72	0.89	1.30	2.24	0.62
	10b	0.0110	0.0089	548.1	1.70	0.91	1.26	2.15	0.61
	50a	0.0099	0.0084	649.1	1.78	0.96	1.27	2.26	0.65
	50b	0.0097	0.0079	663.7	1.84	0.92	1.31	2.40	0.69
	350a	0.0092	0.0071	705.6	1.96	0.86	1.35	2.61	0.77
	350b	0.0100	0.0076	629.3	1.90	0.85	1.36	2.58	0.73
	5000a	0.0094	0.0074	676.4	1.86	0.81	1.22	2.27	0.71
	5000b	0.0108	0.0081	564.1	1.84	0.89	1.48	2.72	0.69
III	10a	0.0257	0.0224	267.0	1.92	1.24	1.59	3.03	0.74
	10b	0.0231	0.0204	310.2	2.00	1.48	1.88	3.75	0.79
	50a	0.0229	0.0191	306.5	2.06	1.06	1.50	3.10	0.83
	350a	0.0221	0.0186	326.6	2.12	1.17	1.64	3.48	0.87
	5000a	0.0224	0.0178	313.1	2.24	1.16	1.84	4.12	0.94
	5000b	0.0230	0.0198	314.2	2.08	1.09	1.46	3.04	0.84

Figure 24

Corrected Loss Factor $\delta''_{\frac{1}{2}}$
at 1000 Cycles $Sec.^{-1}$ and 75° C. vs. Density

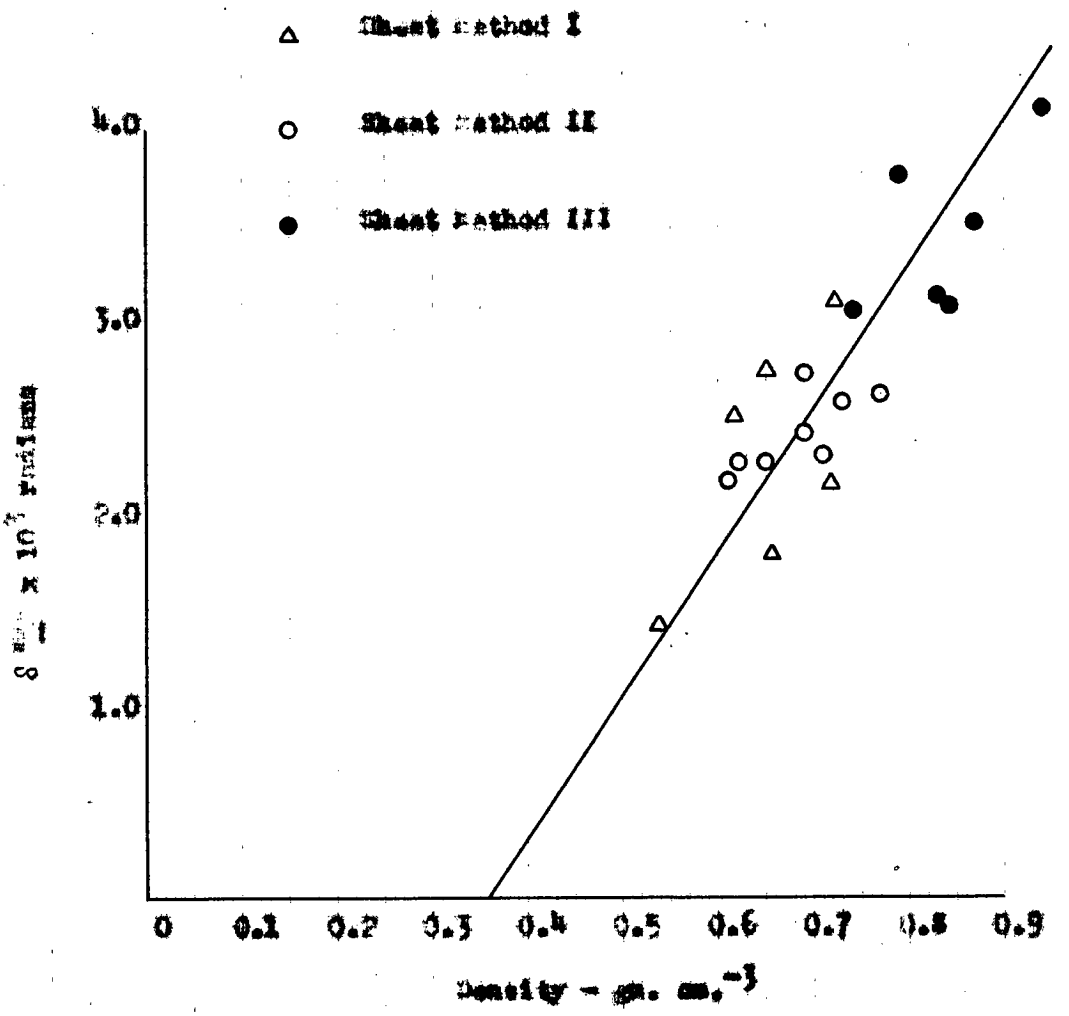

the temperature was reduced as pumping continued, the loss angle increased. It is for this reason that measurements of δ and C_p were reported at 70° C. An attempt was made to determine whether there is a bona fide temperature effect, or whether the increase in δ is due to an increased absorption of water vapor by the sample from the low pressure atmosphere in the test chamber at lower temperatures.

To investigate this phenomenon, a sheet prepared by Method III at 50 p.s.i. pressing was placed in the test chamber and pumped to equilibrium at 70° C. with atmospheric air surrounding the test chamber for Experiment I. After the equilibrium value of δ had been measured at 70° C., the temperature of the test chamber was lowered in several steps to room temperature and δ measured for each step, allowing 2 hours for the attainment of temperature equilibrium. After the room temperature value of δ had been recorded, the test chamber was reheated in steps to 70° C. and δ again measured for each step, allowing 2 hours for the attainment of temperature equilibrium.

For Experiment II the same procedure was followed, except that an atmosphere of air, desiccated by bubbling through concentrated sulfuric acid and then passing over calcium chloride, surrounded the test chamber in the shield.

For Experiment III a moat of water was constructed around the gasket seal of the bell cover in the test chamber and δ determined at various temperature steps, as for Part I.

At the conclusion of these three experiments, the sheet was

removed from the test chamber, and $\underline{\delta}$ and $\underline{t}$ measured as required for the computation of δ' and $\underline{F}'$. The results are given in Table IX and plotted in Figure 25. In Experiment II the sample shifted slightly, giving a different value of $\underline{G}_p$ than that obtained in Experiments I and III. δ' for Experiment II was calculated on the basis that $\underline{F}'$ had not changed, so that a corrected $\underline{\delta}$ for Experiment II could be used in the computation of δ'. All the loops in Figure 25 are read beginning at the lowest point to the right and passing clockwise around the loop.

A slightly higher initial temperature was obtained in Experiment II using the desiccated air, evidently because of the increased heat conductivity of the shield box to the test chamber as a result of circulating dry air inside the shield. The lower initial temperature obtaining in Experiment III was due to the evaporation of water from the mast and to the necessity of removing the shield box from time to time to replace the water which had evaporated.

The idea behind the use of atmospheric air and desiccated air surrounding the test chamber and the water seal surrounding the gasket seal was to produce wide variations in the partial pressure of water vapor inside the test chamber for the three runs. The best pressure maintained by the pump in this series of experiments was on the average about 8 microns of mercury. Because of the continuous flushing action of small amounts of gas admitted by leaks in the test chamber, the partial pressure of water vapor in the test chamber was probably very small in Experiment II, using the desiccated air. In Experiment I, using atmospheric air, the partial pressure of water vapor inside the

TABLE IX

DATA FOR THE CALCULATION OF LOSS ANGLE-TEMPERATURE HYSTERESIS LOSS AT 1000 CYCLES SEC.$^{-1}$

(50 p.s.i. Pressing - Sheet Method III. Two hours between points)

Experiment I - Atmospheric Air

Temperature ° C.	$\delta \times 10^3$ radians	$\delta' \times 10^3$ radians
67	1.15	1.86
51	1.18	1.91
38	1.31	2.12
25	1.50	2.43
36	1.58	2.56
49	1.43	2.32
64	1.26	2.04

Experiment II - Desiccated Air

71	1.17	1.83
55	1.27	1.99
47	1.32	2.06
27	1.49	2.32
40	1.57	2.41
52	1.42	2.22
72	1.23	1.93

Experiment III - Water Seal

62	1.32	2.14
49	1.34	2.17
37	1.41	2.28
25	1.63	2.64
36	1.67	2.71
50	1.60	2.59
61	1.36	2.21

Experiment	$\frac{d}{}$ cm.	$\frac{t}{}$ cm.	$\underline{K}'$	$\underline{C}_p$	δ'/δ
I and III	0.0225	0.0180	2.30	320.0	1.62
II	0.0224	0.0180	2.30	330.0	1.56

Figure #5

Hysteresis Loss Angle - Temperature Loops
at 1000 Cycles Sec.$^{-1}$

(50 psi. Pressing - Sheet Method III.
Two Hours Between Points)

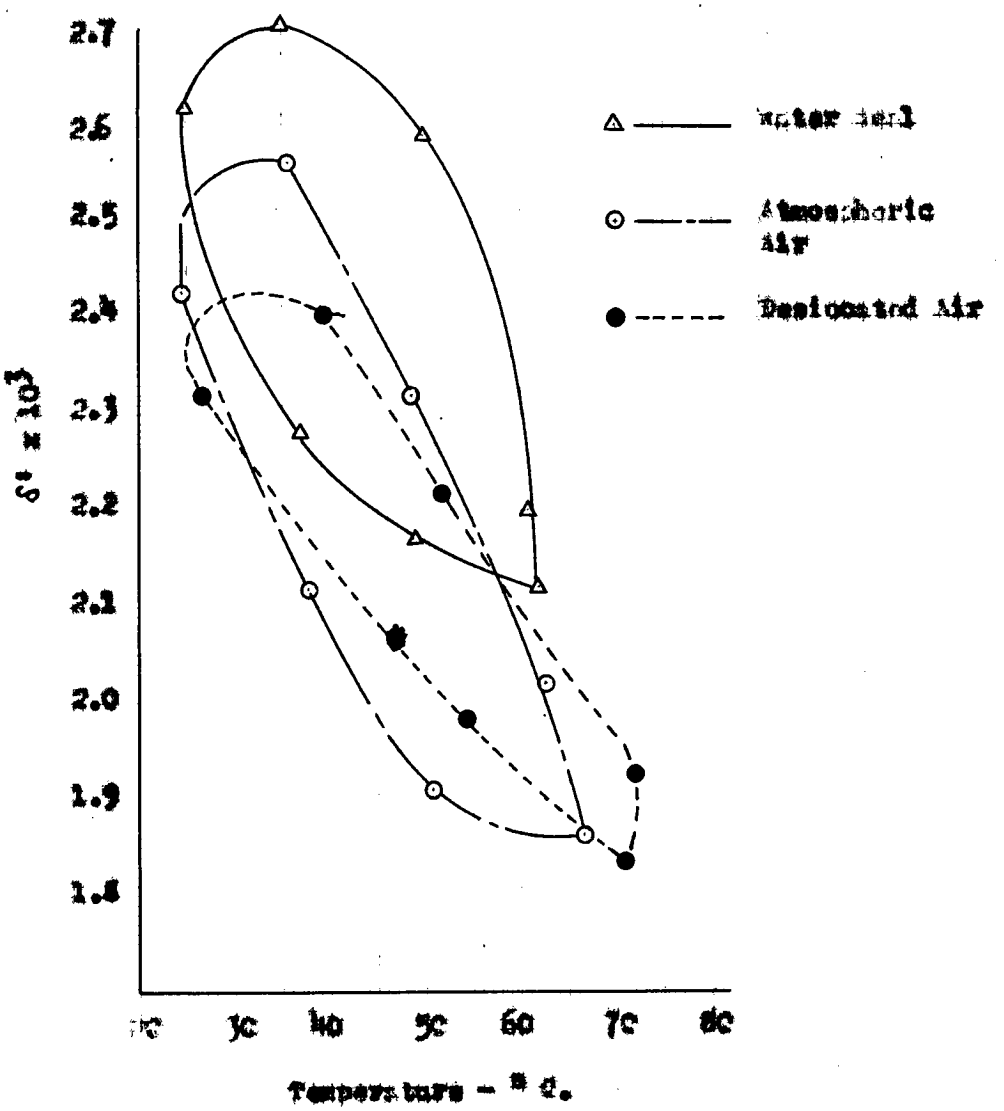

test chamber would be of the order of 0.2 micron of mercury. For Experiment III, using the mass of water surrounding the gasket seal, it is assumed that most of the leakage occurs at this point and, therefore, the greater portion of the pressure of 5 microns of mercury in the test chamber was due to water vapor.

Because it is an established fact that the loss angle δ' of a sheet increases with moisture content and that cellulose has a greater affinity for water vapor at lower temperatures, an increase in δ' is to be expected as the temperature is decreased, the magnitude depending on the partial pressure of water vapor present in the test chamber. If there is no superimposed temperature effect, one would expect a family of loops as shown in Figure 26. With increasing partial

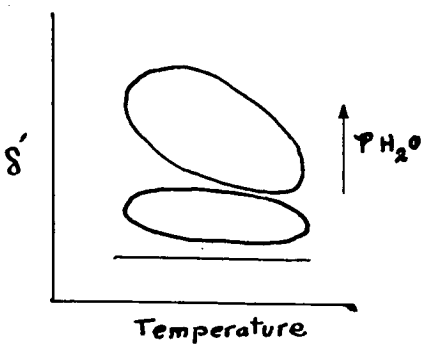

Figure 26

pressures of water vapor the area of the loop would increase, the axis of the loop would have a greater negative slope, and the loop would assume a higher position. If, in addition, there is a bona fide temperature effect, a negative temperature coefficient of δ' would rotate the axis of the loops clockwise and a positive temperature coefficient of δ' would rotate the loops counterclockwise.

Whether or not there is a bona fide temperature effect is difficult to conclude from the family of loops shown in Figure 25. Undoubtedly, the increase in δ' with a decrease in temperature is due, at least in part, to the absorption of water vapor present in the test chamber by the sample, as indicated by the fact that the loops become larger in area and assume a higher position with increasing partial pressures of water vapor in the test chamber.

CONCLUSIONS

A modified alternating-current Schering bridge, together with auxiliary apparatus, was constructed for measuring the dielectric constant and dielectric loss angle of paper. To adapt the apparatus to measurements on paper samples, two special features were included: (1) the chamber containing the test capacitor and guard ring could be evacuated to pressures of a few microns and heated to elevated temperatures for drying the paper to constant electrical properties; (2) to facilitate drying further, the test electrodes could be separated in vacuo during the drying period and brought together for making electrical measurements.

It is necessary to know the separation of the test electrodes when the sample is in place. To do this, a separation gage was constructed having a sensitivity of 3×10^{-5} cm.

A paper sheet will not completely fill a capacitor whose electrodes are plane surfaces, because paper surfaces are by nature irregular. To correct this, a theory was developed to calculate the dielectric constant and loss angle for a sample which does not completely fill a parallel plate capacitor.

The loss angle of paper decreases as drying proceeds. In the capacitance curve versus pumping time (Figure 21), a marked rise in capacitance is noticed as the equilibrium value of the loss angle is approached. This phenomenon can be attributed to an increase in the dielectric constant or to a decrease in the electrode separation

resulting from hygroexpansive changes in the sheet; however, data are not available on this point.

Periodical flushing of the test chamber with a dry, inert gas during the drying period seemed to hasten slightly the attainment of equilibrium. The flushing technique is expected to be more effective in an absolutely airtight apparatus than in one with a minute leak, such as was employed in this investigation.

A hysteresis of the loss angle with ascending and descending drying temperature was noted. It is difficult to conclude positively from the data obtained whether there is a bona fide change of loss angle with temperature, but undoubtedly the increase of the loss angle with a decrease in temperature is due, at least in part, to the absorption of very small amounts of water vapor present in the test chamber.

The greater part of the experimental work of this thesis was concerned with an investigation of the effect of density on the dielectric constant and loss angle of paper. At a given frequency and temperature, the Clausius-Mosotti function states that the expression $(K - 1)/(K + 2)$, where K is the dielectric constant, is proportional to the density of the dielectric. The expression $(K - 1)/(K + 2)$ reduces to zero at zero density, because the dielectric constant of a vacuum is chosen as unity. However, from the experimental data obtained, it was found that the Clausius-Mosotti function did not hold rigorously for paper. The expression $(K - 1)/(K + 2)$ was a straight line; this is in accordance with the theory, but the curve extrapolated

to zero at a sheet density of 0.3 g. cm.$^{-3}$. It is suggested that errors in the values of the electrode separation and the thickness of the sheet used in the computations might be responsible for the departure from the Clausius-Mosotti function.

At a given frequency and temperature, the relation of the loss factor (the product of the loss angle and the dielectric constant) to density should be a straight line extrapolating to zero at zero density, because the loss angle of a vacuum is zero. Experimentally, the relation was found to be linear, but the loss factor extrapolated to zero at a sheet density of 0.45 g. cm.$^{-3}$. It was believed that the departure from the Clausius-Mosotti function resulting from errors in the values of the electrode separation might be responsible for the discrepancies noted. Corrections were made assuming the Clausius-Mosotti relation, but these changes did not shift the curve so that it passed through the origin.

A further study of several points relative to this investigation might explain some of the difficulties encountered. For instance, a method of measuring the electrode separation in situ, without the necessity of transferring the sample to some external measuring device, would be an improvement over the technique developed. Also, the measurement of the thickness of the sample by the usual caliper method is open to question when applied to work of this type. The application of a more fundamental method for measuring the sheet density, which does not include the measurement of questionable quantities, presents an interesting possibility.

LITERATURE CITED

1. A.S.T.M. Tentative Method D 150-41T. A.S.T.M. Standards 1941 Suppl., Part III:375-405.

2. De Luca, H. A., Campbell, W. Boyd, and Kraus, C., Can. J. Research 16B:273-288(1938).

3. A.S.T.M. Tentative Method D 202-41T. A.S.T.M. Standards 1941 Suppl., Part III:406-425.

4. A.S.T.M. Tentative Method D 149-40T. A.S.T.M. Standards 1940 Suppl., Part III:257-263.

5. Kohman, G. T., Ind. Eng. Chem. 31:807-817(1939).

6. Argue, G. H., and Kraus, C., Can. J. Research 13B:156-166(1935).

7. Whitehead, J. B., and Greenfield, E. W., Elec. Eng. 53:1389-1396 (1934); C. A. 28:7382(1934).

8. Greenfield, E. W., J. Franklin Inst. 222:345-358(1936).

9. Race, H. H., Hemphill, R. J., and Endicott, H. S., Gen. Elec. Rev. 43:492-499(1940).

10. Gerton, C. G., J. Inst. Elec. Eng. 86:369-378(1940); C. A. 34: 7603(1940).

11. Whitehead, J. B., and Greenfield, E. W., Elec. Eng. 53:1498-1503 (1934); C. A. 29:250(1935).

12. McLean, D. A., and Kohman, G. T., J. Franklin Inst. 226:203-220 (1933).

13. Murphy, E. J., and McLean, D. A., Annual Report National Research Council, Conf. on Elec. Insulation, p. 20-21(1939).

14. Seborg, C. O., and Stamm, A. J., Ind. Eng. Chem. 23:1271-1275(1931).

15. Weidmann, Fritz, Kunststoffe 29:133-136(1939).

16. Whitehead, J. B., Elec. Eng. 59:660-663(1940); C. A. 35:1540(1941).

17. Vogel, Wilhelm, Papier-Fabr. 37:117-123, 127-132(1939).

18. Piper, John D., Kerstein, M. A., and Kleiger, A. G., Ind. Eng. Chem. 29:1040-1043(1937).

19. Shanklin, H. B., Gen. Elec. Rev. 39:370-372(1936).

20. McLean, D. A., Ind. Eng. Chem. 32:209-213(1940).

21. Finch, J. N., Ind. Eng. Chem. 32:1021-1027(1940).

22. Komagata, S., Trans. Electrochem. Soc. 73:511-521(1938).

23. Hartshorn, L., and Rushton, E., J. Inst. Elec. Eng. 83:315-332 (1938); C. A. 33:774(1939).

24. Stoops, W. N., J. Am. Chem. Soc. 56:1480-1483(1934).

25. Hill, Charles F., J. Applied Physics 8:607-613(1937).

26. Campbell, Albert, Proc. Roy. Soc. A78:196-211(1907).

27. R. C. A. receiving tube manual, p. 67, Technical Series RC-14.

28. Bennett, H. The chemical formulary, Vol. 4, p. 396. New York, Chemical Publ. Co., 1939.

29. Savage, G. M., and Ordal, E. John, Science 91:222-223(1940).

30. National Research Council. International critical tables. Vol. 3, p. 385. New York, McGraw-Hill Book Co., 1928.